European Polymer Journal 257 (2026) 115033

Contents lists available at ScienceDirect

European Polymer Journal

journal homepage: www.elsevier.com/locate/europolj

Self-assembly and polymerization of a molecular switch based on the benzofulvene structure

Alessandro Donati [a], Claudia Bonechi [a], Jacopo Venditti [a], Marco Paolino [a], Mario Saletti [a], Germano Giuliani [a], Gianluca Giorgi [a], Giuseppa Mercorillo [b], Filippo Samperi [b], Chiara Botta [c], Andrea Cappelli [a,*]

[a] Dipartimento di Biotecnologie, Chimica e Farmacia, Università Degli Studi di Siena, Via Aldo Moro 2, 53100 Siena, Italy
[b] Istituto Per i Polimeri, Compositi e Biomateriali (IPCB) U.O.S. di Catania, CNR, Via Gaifami 18, 95126 Catania, Italy
[c] Istituto di Scienze e Tecnologie Chimiche "G. Natta" - SCITEC (CNR), Via A. Corti 12, 20133 Milano, Italy

ARTICLE INFO

Keywords:
Spontaneous polymerization
Topochemical polymerization
π-stacked polymers
Molecular switches

ABSTRACT

In the search of new molecular switches structurally related to Green Fluorescent Protein (GFP) chromophore and based on a 3-phenylbenzofulvene scaffold, we found that some of them were stable in the ordered crystalline state, but in the disordered amorphous state, PEGylated derivative ethyl (*E*)-6-[2-[4-(2,5,8,11,14,17,20,23,26,29-decaoxatriacontyl)-1*H*-1,2,3-triazol-1-yl]ethoxy]-1-(2-oxopyrrolidin-3-ylidene)-3-phenyl-1*H*-indene-2-carboxylate [(*E*)-**VC1801**] underwent spontaneous polymerization leading to random co-polymer materials with molecular oxygen, but containing homo-polymer sequences. Thus, NMR spectroscopy and dynamic light scattering techniques were employed to gain information about the self-assembly process of (*E*)-**VC1801** in the relatively disordered state in which polymerization occurs, and the results highlighted the importance of the aromatic specific interaction in the aggregation process. Very interestingly, the study of the interaction of benzofulvene derivative (*E*)-**VC1801** with light revealed that UV excitation could induce photochemical reactions in the solid state with the formation of new species showing increased emission features. The analysis of the irradiated films showed that along with the photoisomerization reaction of (*E*)-**VC1801** into the corresponding (*Z*)-**VC1801**, also a polymerization process occurred. Intriguingly, the polymerization reaction was more efficient in the presence of atmospheric oxygen than in the sample irradiated under reduced oxygen content, and the photophysical features of the corresponding polymeric materials were significantly different. These differences in the emission features supported the existence of differences in the composition of the samples such as their content in homo-polymer sequences.

Introduction

The development of synthetic strategies focused on the preparation of single crystals of large-size polymer has recently received a great deal of attention [1–7]. In general, topochemical polymerization strategies are based on monomers able to self-organize into ordered structures (in solid-state and/or in solution) through the formation of weak intermolecular non-covalent interactions such as hydrogen bonding, π-π stacking, CH-π, and hydrophobic interactions [8–12].

The concept of topochemical polymerization was related in our laboratories to the spontaneous polymerization of 3-phenylbenzofulvene derivatives (i. e. 6-MO-**BF3k** in Fig. 1) [13–39].

These compounds represented intriguing examples of monomers able to polymerize spontaneously in the solid-state and in highly concentrated solutions in the apparent absence of any catalysts and/or initiators. The interpretation of the results of these studies led to the development of a mechanistic hypothesis, which we called "affinity polymerization" [19,23,33]. Within this hypothesis, we assumed that π-π stacking interactions among the monomers could play a pivotal role in the initial process of affinity recognition preluding spontaneous polymerization.

The so-called light-driven molecular switches (LDMSs) are chemical entities able, as a result of a light stimulus, to interconvert between at least two different isomeric structures, which are characterized by distinct absorption features [40,41]. Thus, in the aim of converting light into mechanical motion, a great design effort has involved both isolated

* Corresponding author.
E-mail address: andrea.cappelli@unisi.it (A. Cappelli).

https://doi.org/10.1016/j.eurpolymj.2026.115033
Received 14 April 2026; Received in revised form 14 July 2026; Accepted 17 August 2026
Available online 19 August 2026
0014-3057/© 2026 The Author(s). Published by Elsevier Ltd. This is an open access article under the CC BY license (http://creativecommons.org/licenses/by/4.0/).

molecules and 2D ordered supramolecular structures [42–52]. For instance, in overcrowded olefins, [53,54] light energy produces the rotation of a part of the molecule with respect to the remaining portion through the isomerization of an exocyclic double bond [55]. A great number of investigations was devoted to regulate the speed of the rotation, [53–55] the absorption features, [56,57] and the quantum yield of isomerization [58]. Moreover, other research efforts were focused on increasing the stability of the photoswitches, [59] on evolving from photoswitches to light-driven molecular rotors, [60,61] and on modulating the solubility in different solvents [62–64].

Within this research topic, our efforts were focused on the design, synthesis, and computational characterization of new LDMS mimicking the behavior of the retinal chromophore within the rhodopsin pocket [65–69] or the structure of the Green Fluorescent Protein (GFP) fluorophore (Fig. 1) [70–72].

Recently, we reported on GFP-like chromophores based on a 3-phenylbenzofulvene scaffold **VC1775** and **VC1801**, which were demonstrated to absorb visible (blue) light (in their neutral form) and to photoisomerize in the picosecond time scale [73]. Moreover, PEGylated derivative **VC1801** showed the propensity to self-assemble in water at

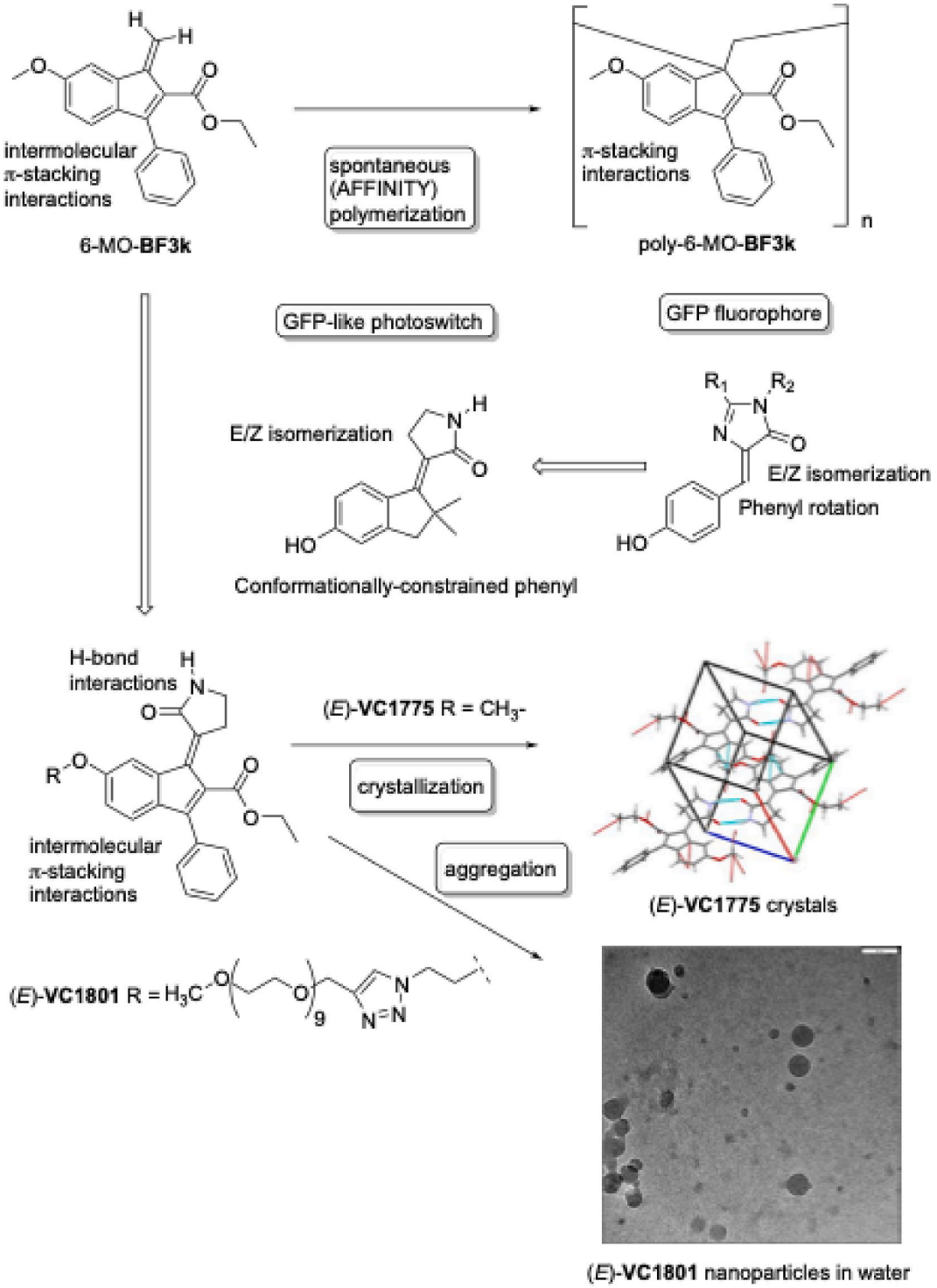


Fig. 1. Structures of some benzofulvene derivatives.

the concentrations above its critical aggregation concentration (CAC) with the formation of several heterogeneous populations of nano-aggregates. In particular, populations showing small mean diameters (from 3 to 10 nm) were present along with other components showing greater dimensions (around 30 and 200 nm), and aggregation appeared to affect the photochemical features in the aqueous environment [73].

In the present paper we show that while simple benzofulvene derivative **VC1775** was stable in the ordered crystalline state, PEGgylated derivative **VC1801** appeared to undergo spontaneous polymerization in the disordered amorphous state. Thus, the spontaneous polymerization process was investigated in terms of its possible mechanism and the role of factors such as aggregation state, interaction with light, and presence/absence of molecular oxygen.

Results and discussion

Spontaneous polymerization of VC1801

3-Phenylbenzofulvene molecular switch (*E*)-**VC1801** was resynthesized in a number of different batches by following the already published procedure [73]. These successful experiments allowed us to demonstrate the robustness of the synthetic procedure and to further optimize it.

Compound (*E*)-**VC1801** was stored as a red–orange glassy solid in closed vial at room temperature and was initially demonstrated to be stable in these conditions. This stability and the consequent apparent lack to the tendency toward the spontaneous polymerization typical of the benzofulvene derivatives was explained with the presence of the bulky pyrrolidinone moiety directly attached to the exocyclic double bond usually involved in the spontaneous polymerization. However, during the advancement of the characterization studies we observed the progressive formation of polymeric materials in the vials containing the more recently synthesized lots of (*E*)-**VC1801**. Thus, the early synthesized batches were analyzed by NMR spectroscopy, which confirmed the occurrence of the spontaneous polymerization in the solid state. As expected, the ^{1}H NMR spectrum of a poly-**VC1801** sample obtained by spontaneous polymerization in the solid state showed broad signals (Fig. 2), which were up-field shifted with respect to those present in the spectrum of the corresponding monomer (*E*)-**VC1801**, supporting the polymeric nature of the poly-**VC1801** sample.

Moreover, the structure of the broad signals and the lack of signals at around 9 ppm suggested the presence of oligomeric species in which the polymerization mechanism involved the exocyclic double bond connecting the pyrrolidinone moiety to the indene one. In fact, the presence of a signal at around 9 ppm in the spectrum of monomer (*E*)-**VC1801** was explained with the coplanarity of the pyrrolidinone ring with the indene moiety that placed the aromatic H-7 proton in the deshielding cone of the pyrrolidinone carbonyl group as suggested by the structure of (*E*)-**VC1775** obtained by crystallographic studies [73]. The apparent lack of broad signals in the aromatic region at around 9 ppm was interpreted with the deplanarization of the pyrrolidinone-indene system because of the break of the exocyclic double bond (i. e. the change in hybridization from sp2 to sp3) occurring during the oligomerization process.

The comparison of the corresponding ^{13}C NMR spectrum (Fig. 3), showing a better resolution, further supported our assumption about the polymeric nature of the poly-**VC1801** sample obtained by spontaneous

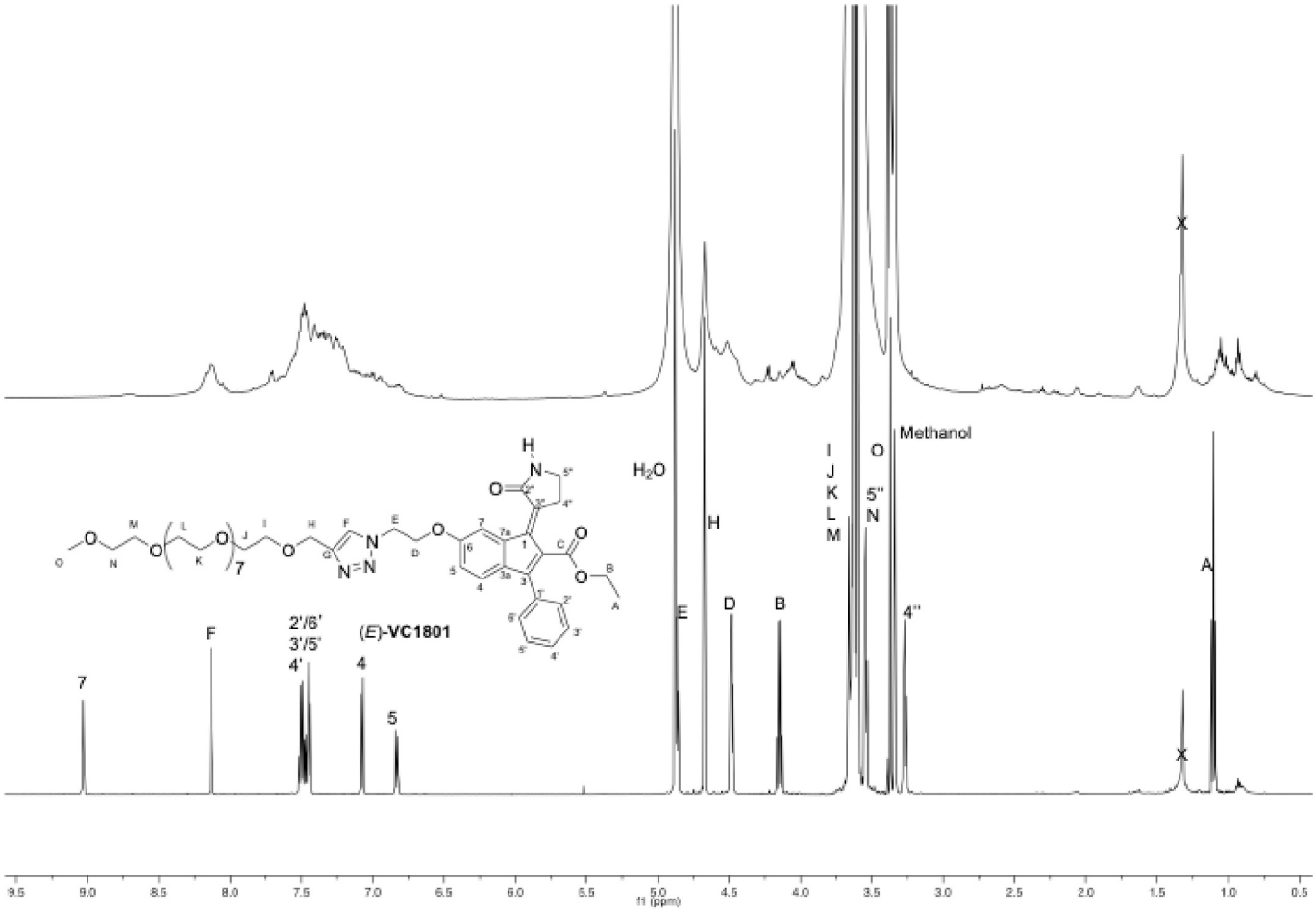


Fig. 2. Comparison of the ^{1}H NMR spectrum (CD_3OD, 600 MHz) of the poly-**VC1801** sample obtained by spontaneous polymerization in the solid state (top trace) with that of corresponding benzofulvene derivative (*E*)-**VC1801** (CD_3OD, 600 MHz, bottom trace).

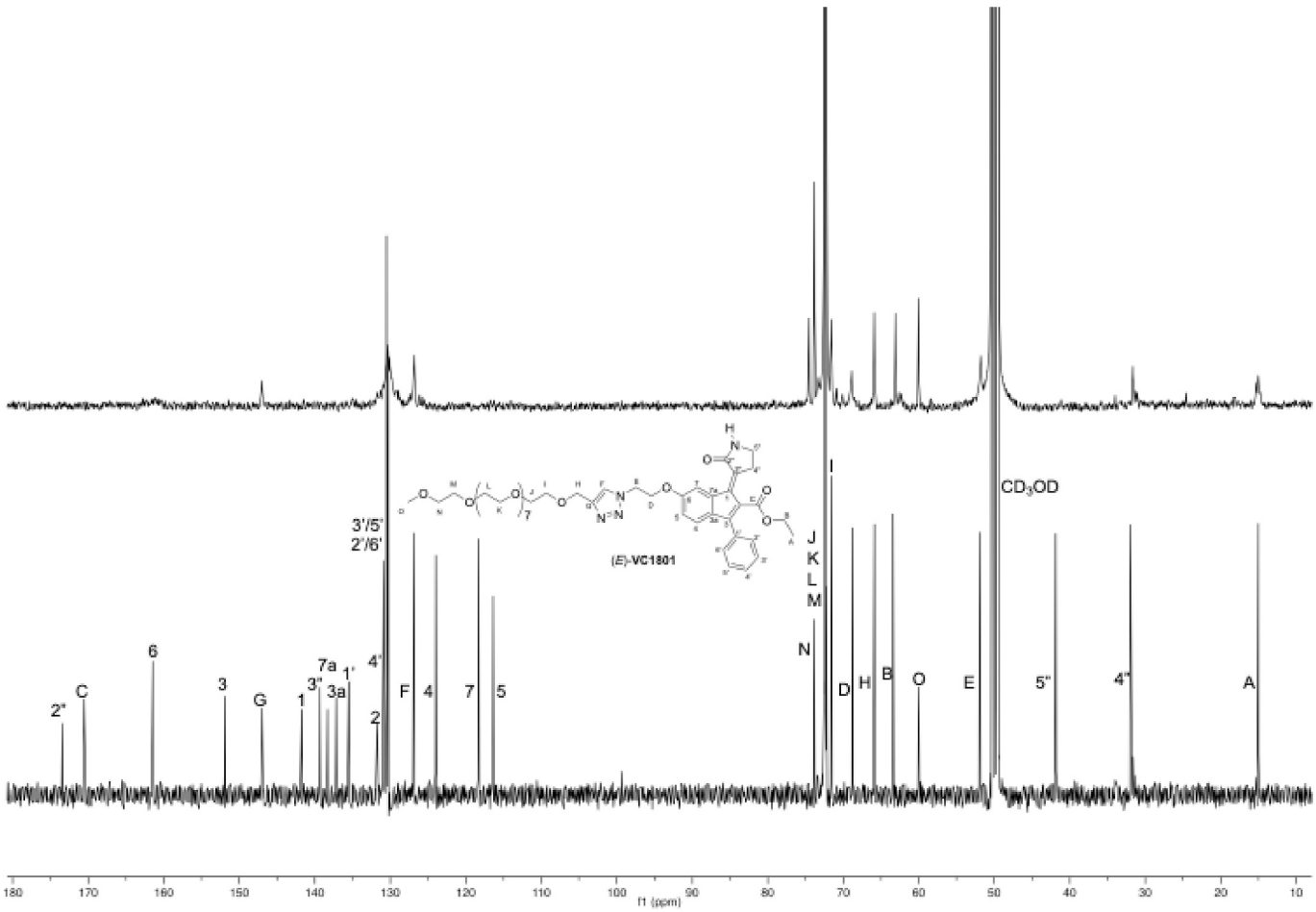


Fig. 3. Comparison of the ^{13}C NMR spectrum (CD_3OD, 150 MHz, top trace) of the poly-**VC1801** sample obtained by spontaneous polymerization in the solid state (top trace) with that of the corresponding benzofulvene derivative (*E*)-**VC1801** (CD_3OD, 150 MHz, bottom trace).

polymerization in the solid state.

However, the quality of ^{13}C NMR spectrum was insufficient to gain significant information about the structure of poly-**VC1801**. Thus, MALDI-TOF mass spectrometry experiments were performed to obtain the necessary relevant structural information. The best mass spectrum was recorded in reflectron mode using malononitrile as the matrix and is displayed in Fig. 4.

The MALDI-TOF mass spectrum shows a series of significant peaks at *m/z* values of around 935, 951, 953, 967, 969, and 987 Da with intervals corresponding to the mass of oxygen atoms. Thus, the monomeric unit of the poly-**VC1801** could bear one, two, three, or four oxygen atoms producing sodiated ions at the mass peaks 935.6, 951.6, 967.6 and 983.6, respectively. Moreover, similar patterns were observed at higher molar mass values corresponding to dimers and trimers. Table 1SI (see Supporting information) shows the calculated and experimental masses of the oligomeric species observed. Therefore, on the bases of the MALDI-TOF mass data we assumed that poly-**VC1801** sample obtained by spontaneous polymerization in the amorphous solid state (i. e. transparent thick film) was a copolymer with molecular oxygen (−O–O–) linked to the polybenzofulvene monomeric units. Our findings suggested that the covalent bond between carbon and peroxide units (C-O-O-) in the backbone of polybenzofulvene chains was labile during the desorption and ionization processes occurring in MALDI-TOF MS analysis, as previously observed by Nakano et al. in a copolymer consisting

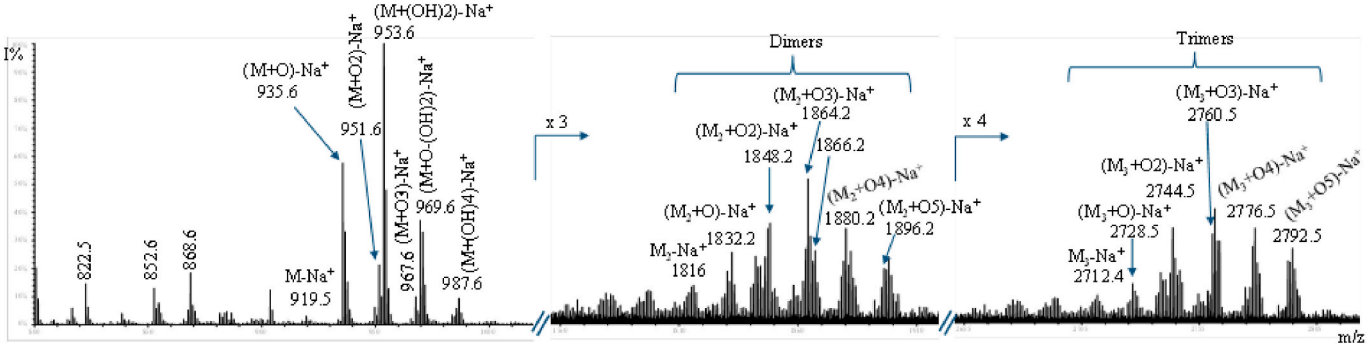


Fig. 4. MALDI-TOF mass spectrum of the poly-**VC1801** sample obtained by spontaneous polymerization in the solid state recorded in reflectron mode using malononitrile as a matrix.

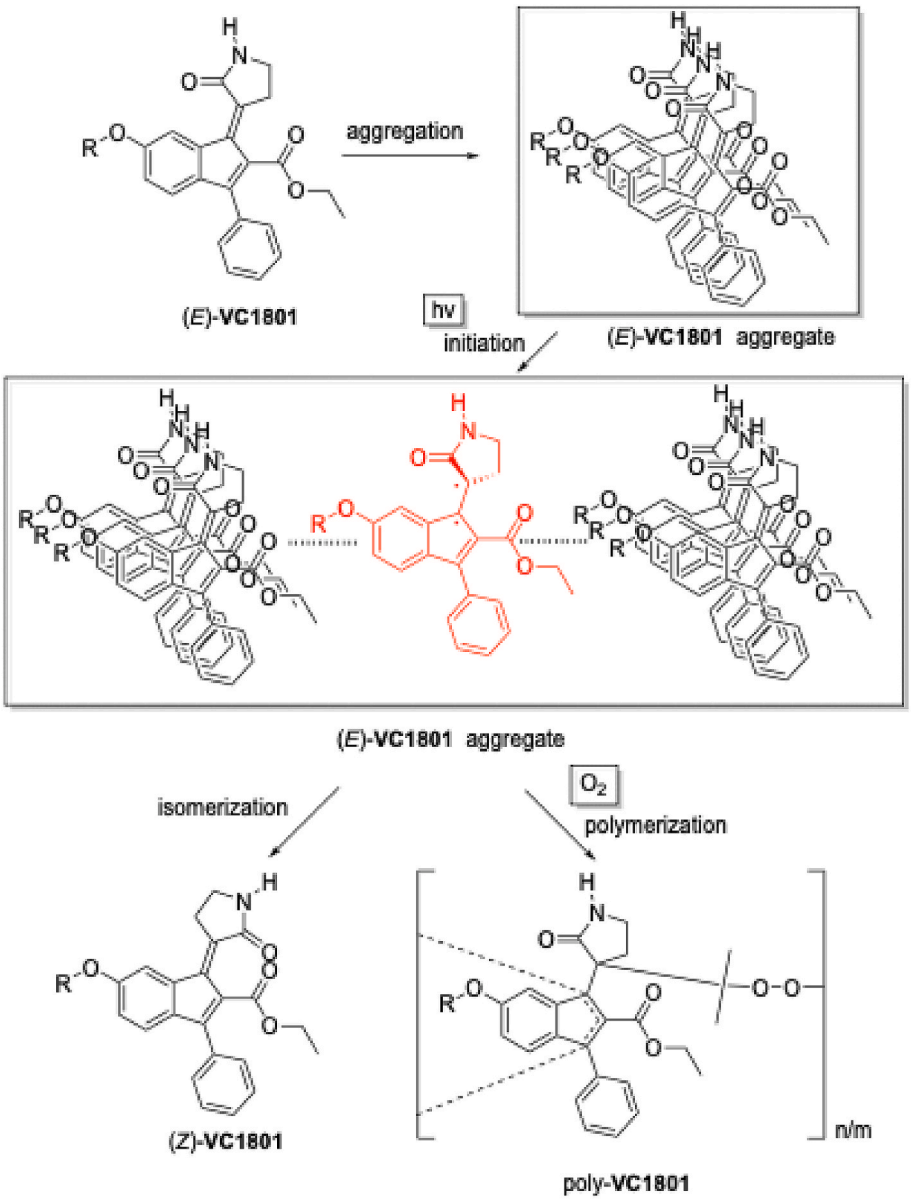
of dibenzofulvene (DBF) and molecular oxygen (−O−O−) units [74]. In agreement with the results obtained by Nakano et al., the analysis of the peak patterns corresponding to dimeric and trimeric species revealed the existence of non-oxidized homo-polymeric sequences and of sequences showing low oxygen contents. These results led us to assume for poly-**VC1801** obtained by spontaneous polymerization the structure of a random co-polymer with molecular oxygen containing homo-polymeric sequences along with those of the alternate co-polymer. The presence of the peroxide bonds (−O−O−) along the chains was confirmed by FT-IR spectroscopy, which showed peaks at 1130, 1000, and 870 cm^{-1} (Fig. 1SI, see Supporting information) attributed to the stretching of these moieties. The broad peak between 3300 and 3500 $cm^{-1}$was assigned to the stretching of the –OH and −O-OH functional groups.

To further evaluate its polymeric nature, the poly-**VC1801** sample obtained by spontaneous polymerization in the solid state was characterized by size exclusion chromatography (SEC) (Fig. 2SI), using THF as the eluent (1 mL/min). The analysis of the SEC trace (Fig. 2SI) confirmed that the poly-**VC1801** sample obtained by spontaneous polymerization in the solid state was constituted by low molar mass oligomers in agreement with the results obtained by NMR studies and MALDI-TOF measurements. An average number molecular weight (Mn) of about 2300 g/mol was calculated by applying the calibration curve build with polystyrene standards.

DSC analysis of poly-**VC1801** showed that this polymer presented a glass transition temperature (Tg) at about –22 °C and an endothermic melting process in the range between 30 and 90 °C (Fig. 3SI).

Thus, rather surprisingly, the steric bulk produced by the presence of the pyrrolidinone moiety directly attached to the exocyclic double bond of the 3-penylbenzofulvene scaffold appeared to be compatible with the spontaneous polymerization mechanism (Scheme 1).

We previously assumed that the spontaneous polymerization of benzofulvene derivatives occurs through a two-step mechanism we called “affinity polymerization” [33]. During the first step, the benzofulvene monomers mutually recognize and interact (as in a crystallization process) with the formation of relatively ordered supramolecular systems (i. e. columnar aggregates). The aggregate architecture is determined by the establishment of different short-range interactions (i. e. specific aromatic interactions), and, when the intermolecular distance and the orientation of the monomers are suitable, the polymerization mechanism becomes operative and starts as a domino reaction



Scheme 1. Hypothetical mechanism for the spontaneous polymerization of benzofulvene derivative **VC1801**.

(polymerization step). Thus, the ordered orientation of the monomers within the columnar aggregate could affect the enchainment of the resulting polymer [39].

A pivotal role in the aggregation process, aggregate architecture, polymerization, and polymer features was assumed for the pendant phenyl ring of the 3-phenylbenzofulvene moiety that appeared to be capable of establishing specific aromatic (i. e. T-shaped) interactions [33].

In the case of the spontaneous polymerization of the benzofulvene molecular switch **VC1801**, the presence of molecular oxygen appeared to play a pivotal role in determining the nature of the resulting polymer. In the aggregate state, the biradical intermediate generated by the excited state could be assumed to react with molecular oxygen or with another **VC1801** molecule producing a random co-polymer with molecular oxygen containing homo-polymeric sequences.

Thus, aggregation state, interaction with light, and presence/absence of molecular oxygen could be assumed to play a role in the spontaneous polymerization of **VC1801**.

Aggregation of VC1801

In our previous work, the aggregation features of (*E*)-**VC1801** in water were characterized by pyrene fluorescence analysis, DLS, cryo-TEM, and TEM [73]. Fluorescence analysis with pyrene as the probe allowed us to determine a critical aggregation concentration (CAC) value of 0.069 mg/mL [73]. Rather surprisingly, DLS analysis of a water solution at the concentration value of 0.1 mg/mL (just above its CAC) showed the propensity of (*E*)-**VC1801** to generate several heterogeneous populations of nanoaggregates [73]. The cryoTEM investigations performed on a 10 mg/mL water solution (concentration well above its CAC) confirmed the presence of heterogeneous populations of spherical particles with a large preponderance of small particles showing dimensions in the range 10–80 nm. Finally, TEM investigations performed by negative staining with uranyl acetate on the same sample used in the cryoTEM studies confirmed the presence of heterogeneous populations of spherical particles with a large preponderance of small and very small particles [73].

In order to refine the studies published in our previous paper, [73] DLS measurements were performed in relatively concentrated dispersions (i. e. 4.0, 2.5, and 0.5 mg/mL) well above the critical aggregation concentration. The results (Table 1) confirmed the formation in water of populations showing small mean diameters (from 9-10 nm) along with other components showing greater dimensions (around 83–87 and 360–588 nm) [73].

This heterogeneity was rather surprising and could be rationalized in terms of the presence of multiple supramolecular architectures in the nanoaggregates. In other words, we assumed that the self-assembling process could be driven by two dominant interactions such as π-π stacking interactions among the 3-phenylbenzofulvene aromatic systems and the H-bond interactions between the pyrrolidinone rotating head (seen in the crystal structure of compound (*E*)-**VC1775**). These interactions could play roles of different importance with one being dominant over the other.

Table 1
Mean hydrodynamic diameter and polydispersity index values of the nanoparticles present in the dispersion of **VC1801** in water at room temperature and different concentration values from 4.0 to 0.5 mg/mL.

Concentration (mg/mL)	Mean size ± sd (nm)	Mean size ± sd (nm)	Mean size ± sd (nm)	Polydispersity index (PDI)
4.0	8.81 ± 0.44	83.06 ± 8.25	588.4 ± 26.57	0.678 ± 0.034
2.5	10.72 ± 0.54	82.86 ± 4.14	476.7 ± 21.83	0.598 ± 0.015
0.5	9.34 ± 0.47	86.64 ± 4.33	360.2 ± 18.54	0.490 ± 0.024

Thus, ^{1}H NMR spectra were recorded on the (*E*)-**VC1801** dispersions showing the same concentration values spanning one order of magnitude from 4.0 to 0.5 mg/mL (well above the CAC value) and variable times after the dissolution.

The system underwent aggregation processes leading to large and not well-resolved NMR signals, as it is typical for macrosystems. This behavior was found to be stable and did not change over time. Moreover, in this concentration range well above the CAC value (i. e. 4.0–0.5 mg/mL), the ^{1}H NMR spectra appeared only marginally affected by the concentration value. Thus, this observation taken together with the results obtained from the DLS measurements suggested that the aggregation processes in water did not appear to be affected by the concentration value in the range from 4.0 to 0.5 mg/mL.

The assignment of the ^{1}H NMR signals of (*E*)-**VC1801** spectra in $CDCl_3$, CD_3OD or D_2O was performed by COSY and NOESY experiments and is shown in Table 2SI. 2D NOESY spectra in D_2O were recorded with different mixing times (200, 400, and 600 ms) to highlight the presence of aggregates and to obtain structural information. Indeed, the (^{1}H–^{1}H) NOESY spectrum depends on the tumbling rate of the molecule, which is roughly proportional to the molecular weight, but also depends on its polarity as well as the polarity and viscosity of the solvent. For large molecules, the NOESY cross peaks have the same sign as the diagonal peaks. The NOESY spectrum of (*E*)-**VC1801** (Fig. 4SI) shows that the cross and diagonal peaks have the same sign as for large molecules. These experimental data confirm the presence of aggregates.

From the analysis of the NOESY spectrum it is possible to understand the spatial proximity between protons and their interaction through space. Strong NOE couplings were observed between all aromatic protons (H_7, H_F, $H_{4',5',6'}$, H_4 and H_5) and the other protons of the chain (H_D, H_E, H_B, $H_{I,L}$). The dipolar couplings between the methyl group (H_A) and H_F as well as between H_F and the aromatic protons ($H_{4',5',6'}$) are of fundamental importance to suggest a π-stacking interaction. In particular, the dipolar coupling CH_3-H_A-H_F indicates an anti-parallel stacking interaction.

The presence of aggregates influences the molecular motions in solution, and to study the non-selective relaxation rate R_1^{NS} as a function of temperature allows us to confirm the motion of the system in solution. Fig. 5SI (see Supporting information) shows the R_1^{NS} relaxation rate of the aromatic protons H_E and H_D, which relax with a dipolar relaxation mechanism, as a function of temperature. For both protons, the relaxation rate increases with increasing temperature (range 290–313 K), indicating that the molecular motion characterizing the system is slow ($\omega_0\tau_c > 1$). These experimental data confirm that (*E*)-**VC1801** aggregates in solution and that the aggregate is characterized by slow motion conditions, a behavior similar to that of low molecular weight proteins [75,76].

To obtain information about the behavior of (*E*)-**VC1801** in water at very low concentrations well below the CAC value, ^{1}H NMR spectra (Fig. 5) were performed on the (*E*)-**VC1801** dispersion showing different concentration values spanning more than two orders of magnitude from 5.0 (i. e. well above the CAC value) to 0.01 mg/mL (well below the CAC value).

The comparison shown in Fig. 5 suggested that the self-assembling process involving (*E*)-**VC1801** in water appeared to depend by the concentration. In fact, at very low concentration values (i. e. 0.01 mg/mL) the signals of the aromatic protons appeared to be better resolved. Moreover, a progressive splitting appeared to involve the signals assigned to the protons of the phenyl substituent, suggesting that a possible specific aromatic interaction could drive the aggregation at low concentration. In other words, we assumed that at very low concentration values such as 0.01 mg/mL (well below the CAC value) the phenyl substituent could be able to establish a specific aromatic interaction leading to the formation of very small aggregates, which could be unable to host the pyrene used in the CAC measurements by fluorescence analysis. The idea suggested by Fig. 5 is that the aggregation process involving (*E*)-**VC1801** is present also at very low concentration values

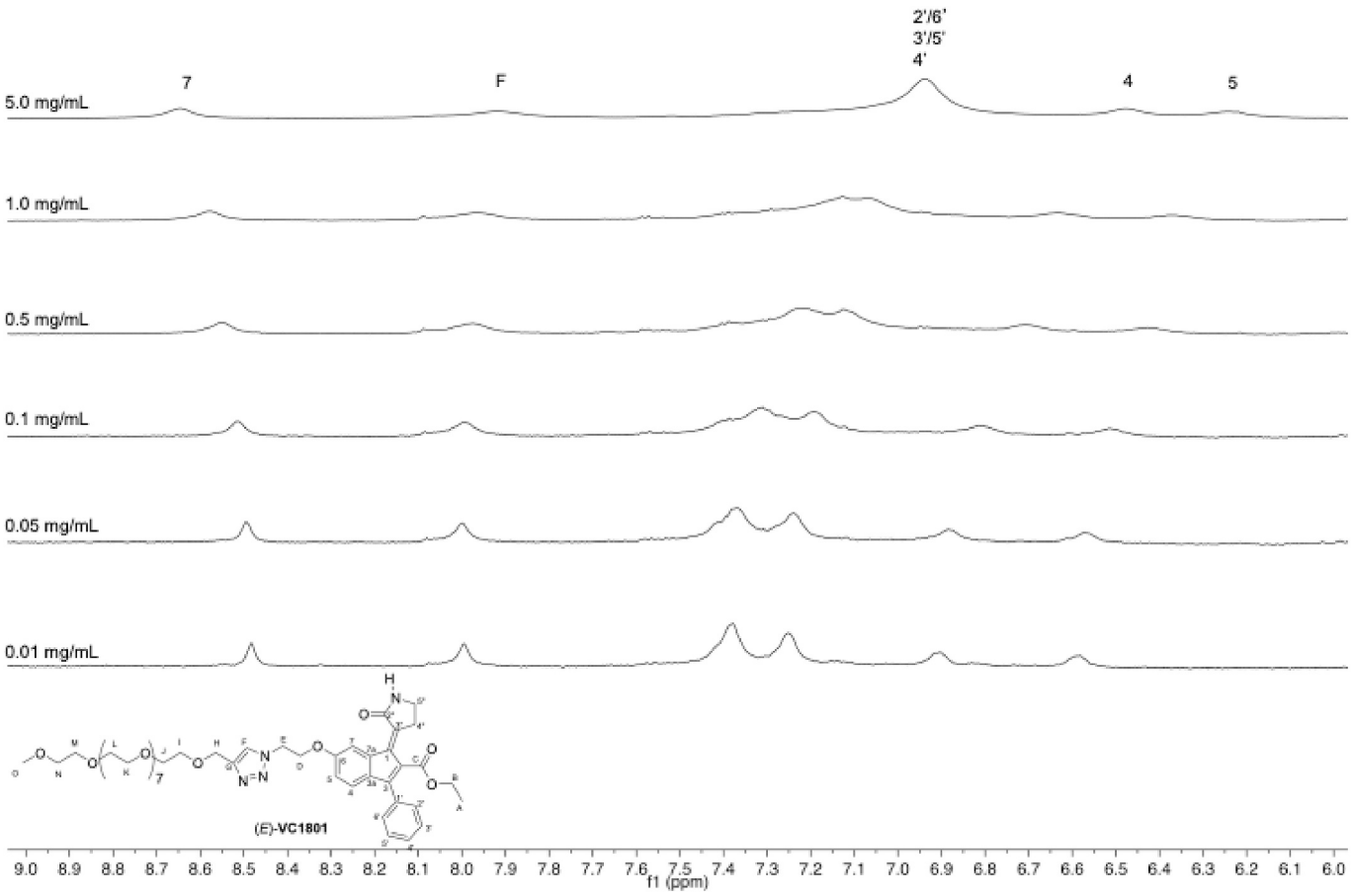


Fig. 5. Comparison of the aromatic regions of the ^{1}H NMR spectra (500 MHz) obtained with water dispersions of (*E*)-**VC1801** showing different concentration values spanning more than two orders of magnitude from 5.0 (top trace) to 0.01 mg/mL (bottom trace).

with the formation of very small aggregates featuring relatively simple architectures based on aromatic specific interactions. These aggregates are capable of growing in architecture complexity and dimensions with the increasing of the concentration up to the formation of the heterogenous system typical of the high concentration values.

It is noteworthy that specific aromatic interactions (i. e. T-shaped) and antiparallel orientation of the bicyclic aromatic nucleus are recurrent motifs in the aggregation and polymerization of the benzofulvene derivatives [16,33].

A similar aggregation behavior was observed also in the methanol–water system (Fig. 6).

The comparison shown in Fig. 6 suggested that (*E*)-**VC1801** was molecularly dissolved in methanol, and the progressive addition of water induced aggregation. The splitting of the signals assigned to the protons of the phenyl substituent is visible just in the presence of small amount of water, where the line broadening suggests the formation of small aggregates. This observation supports the importance of the specific aromatic interaction just in the first phase of the aggregation process involving (*E*)-**VC1801**. Moreover, the specific up-field shifting of the signals assigned to protons 2′/6′ appeared to support their interaction with the π-electron cloud of an aromatic counterpart as expected in a T-shaped specific aromatic interaction.

Interaction of VC1801 with light

The interaction of benzofulvene molecular switch (*E*)-**VC1801** with light was studied in the first instance by assessing its absorption and emission features. As previously reported, [73] diluted methanol solutions of (*E*)-**VC1801** displayed an absorption maximum at 280 nm with a shoulder at about 355 nm and a weaker broad band at 430 nm (Fig. 7, bottom).

Upon irradiation with an UV-A lamp (irradiance 300 μW/cm^2) the absorption spectrum showed a significant reduction of the shoulder at 355 nm, accompanied by the increase in absorbance at 330 nm and 270 nm, with a slight decrease and blue-shift of the 430 nm band, as evidenced by the Δα spectra (Fig. 7, top). On the other hand, the emission of the methanol solution was very weak (broad band centered at 420 nm) and after UV-A irradiation its intensity showed a slight increase (Fig. 6SI).

These results suggested that the optical features of the benzofulvene molecular switch (*E*)-**VC1801** molecularly dispersed in methanol were moderately affected by the irradiation with UV-A light at 365 nm in agreement with the results previously obtained with the closely related (*E*)-**VC1775** [73]. In particular, we previously showed that the irradiation of this latter compound produced the double-bond isomerization in the pico-second scale with the formation of the corresponding (*Z*)-diastereomer showing absorption features very similar to those shown by (*E*)-**VC1801** [73].

Thus, to evaluate the photochemical behavior of (*E*)-**VC1801** in the molecularly dispersed form, its solutions in CD_3OD were irradiated with monochromatic light centered at different wavelengths (i.e. 330, 360, and 460 nm), while ^{1}H NMR spectra were recorded at regular time intervals to ascertain the effects of the irradiation (see Figs. 7SI-9SI).

The kinetic trend of these experiments showed a progressive decrease of the signals attributed to (*E*)-**VC1801** in favor of those attributed to (*Z*)-**VC1801**. As expected, the signal referred to proton 7 underwent a significant change in its chemical shift value from 9.02 ppm to approximately 7.25 ppm due to its exit from the de-shielding cone of

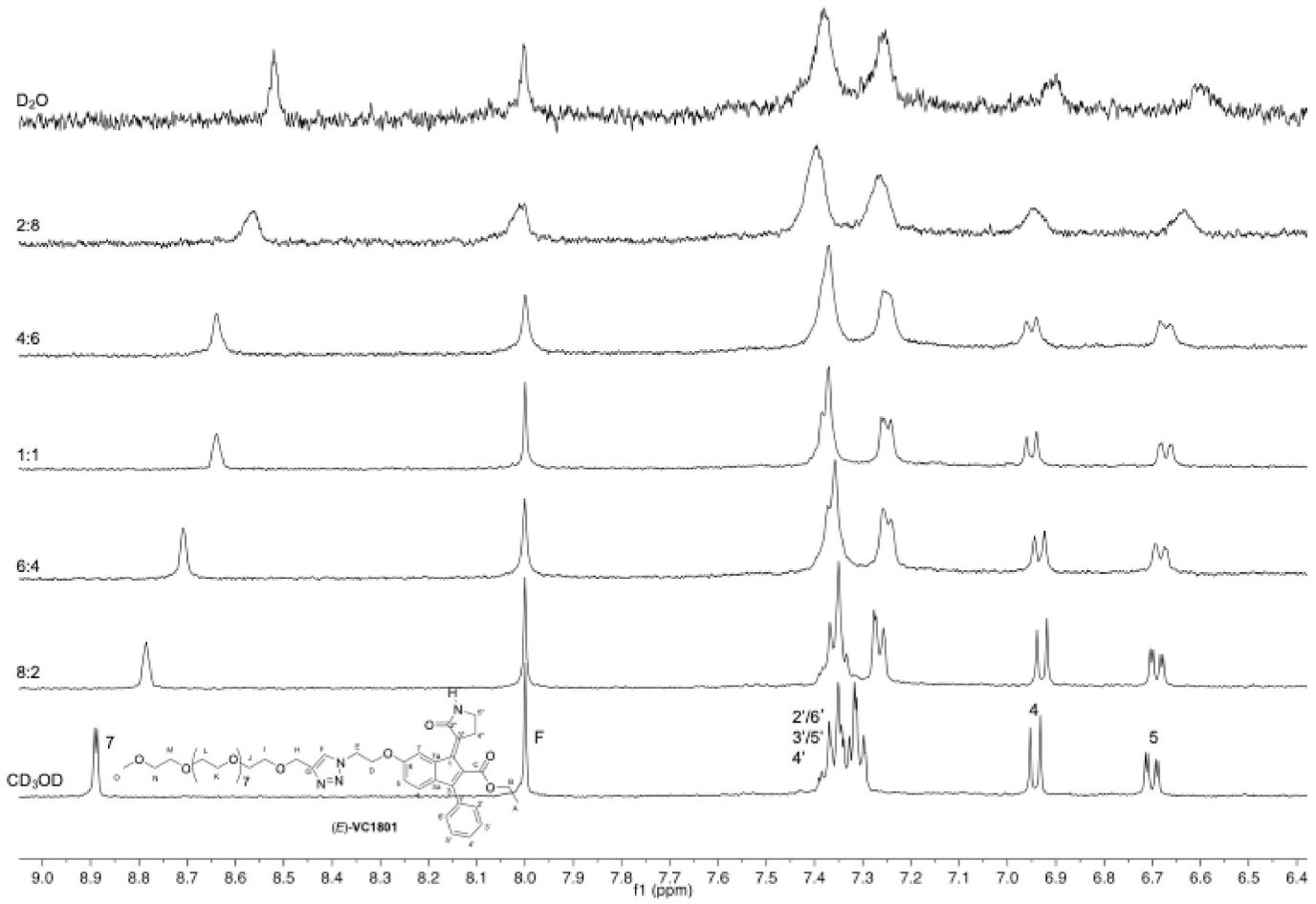


Fig. 6. Comparison of the aromatic regions of the ^{1}H NMR spectra (500 MHz) obtained with dispersions of (*E*)-**VC1801** showing different proportions of water and methanol.

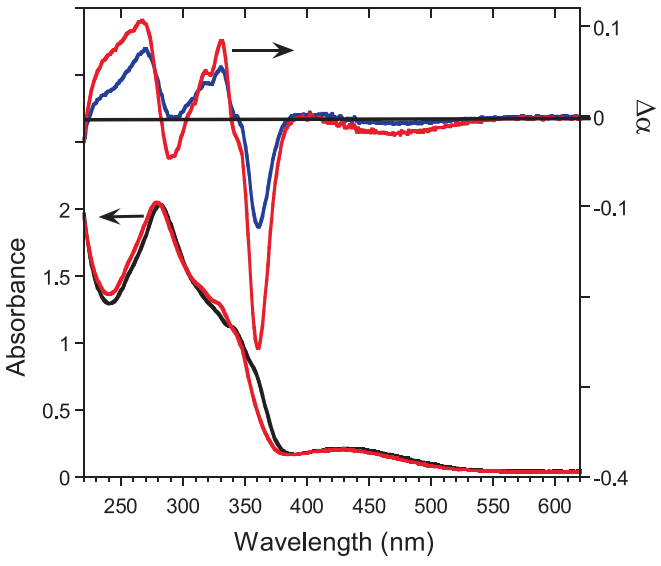


Fig. 7. Absorption spectra (bottom) of a methanol solution of (*E*)-**VC1801** (c = 0.39 mg/mL, cell path 0.5 cm) as prepared (black line) and after 11 h of UV-A irradiation (red line). Top: Absorbance variation Δα of the solution after UV-A irradiation for 1 h (blue line) and 11 h (red line).

the carbonyl group of the pyrrolidinone ring.

Interestingly, in the compositions of the photostationary states (PSS) of derivative **VC1801** (Fig. 8) the *Z* isomer proportion of approximately 66 % obtained after excitation at 360 nm was higher than those obtained after excitation at 330 nm (53 %) and 460 nm (42 %) respectively (see Table 2).

Finally, the PSS solutions were stored at room temperature in the dark for a few days without displaying a significant change in the *E/Z* composition. This behavior suggested the presence of a remarkable interconversion thermal barrier between the two isomers.

Differently from the solutions, (*E*)-**VC1801** in the solid state (i. e. cast films) showed both absorption and emission properties strongly dependent on the UV exposure. In Fig. 9, the absorption spectrum of a cast film of (*E*)-**VC1801** is compared for the pristine film (top) and after exposure to monochromatic (330 nm, 3 mW/cm^2) UV irradiation (bottom) for 150 min.

The film absorption spectrum displays two broad bands at about 290 nm and 460 nm. After UV exposure, the absorbance of the 460 nm band decreases and shifts to 440 nm, while a shoulder at about 360 nm reveals the increase of absorbance in the 330–360 nm region.

Very interestingly, the effect of UV irradiation on the emission properties was impressive. In fact, the very weak emission of the pristine film (broad band at 610 nm) changed during the measurement when UV excitation light was employed, turning into a bright blue emission after few minutes of exposure (Fig. 9 bottom and Fig. 10a). In particular, the growth of two new emission bands (a narrow band at 412 nm and a broad band centered at 550 nm) was observed in the first minutes, displaying a nearly linear growth with the irradiation time in the first hour. The 412 nm band was observed to grow with a faster rate with respect to the 550 nm one, as shown in the inset of Fig. 10a). By exposing

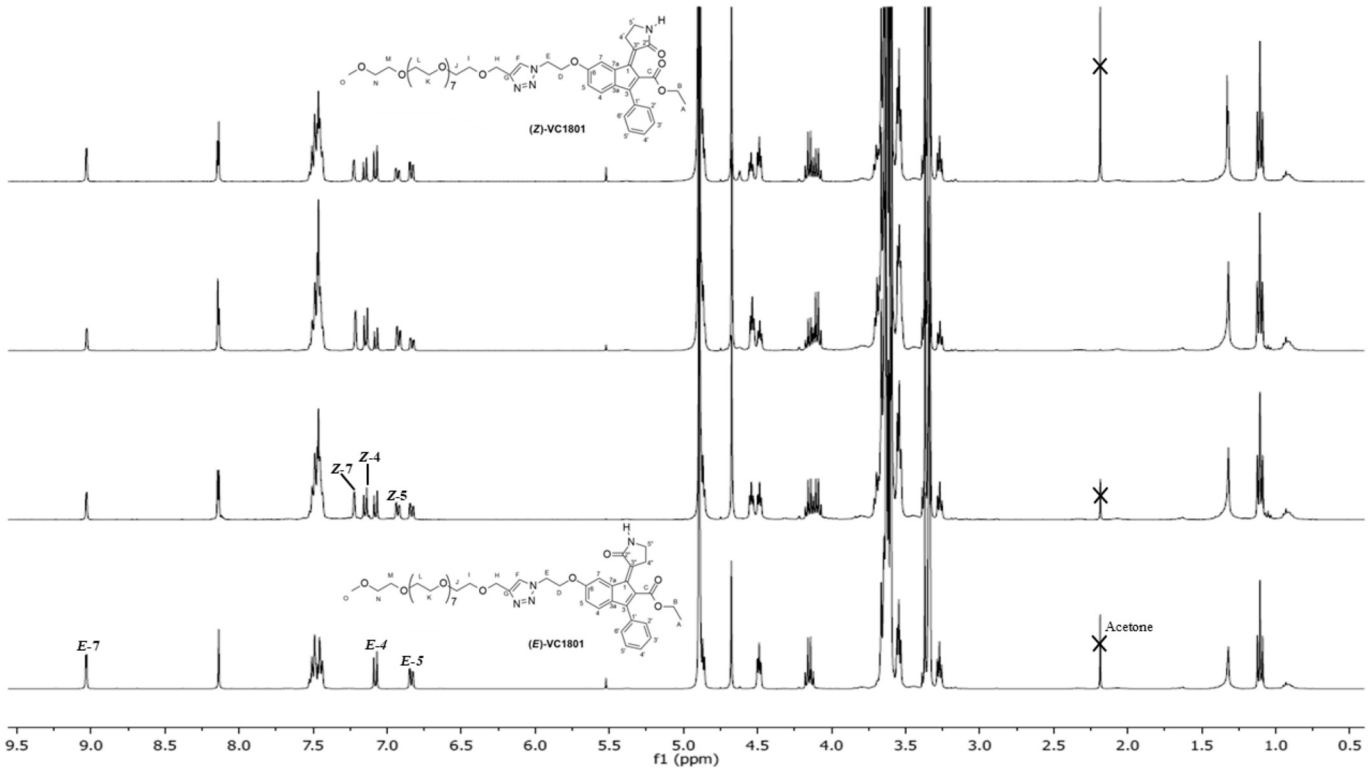


Fig. 8. Comparison of the ^{1}H NMR spectra (400 MHz, CD_3OD) of (*E*)-**VC1801** (bottom trace) with the mixture of the *E* and *Z* isomers at the PSSs reached after irradiation at (from the bottom to the top) 330, 360, and 460 nm.

Table 2
Schematic summary of *E/Z* ratio in the **PSS** composition mixtures obtained during the photoisomerization experiments of (*E*)-**VC1801** in CD_3OD.

330 nm ***E/Z* ratio**	**time required**	360 nm ***E/Z* ratio**	**time required**	460 nm ***E/Z* ratio**	**time required**
48:52	57 h	34:66	120 h	60:40	72 h

the cast film to a second irradiation cycle, the increase of the intensity reached a plateau in about 150 min (see the inset of Fig. 10a).

In summary, as shown in Fig. 10, after 150 min of UV exposure, the main emission of the film was centered at 412 nm (narrow band) and was excited at 330 nm, while a weaker band at 550 nm was selectively excited at 440 nm (Fig. 9 bottom and Fig. 10b). Such a behavior suggests that the UV excitation is able to induce photochemical reactions in the solid state, producing new species, one with emission at 412 nm and one with emission at 550 nm, both possessing increased emission capability with respect to the pristine compound (*E*)-**VC1801**.

To obtain information about the photochemical reactions in the solid state, the effects of the interaction of compound (*E*)-**VC1801** with light in the amorphous solid state (i. e. films) were studied by ^{1}H NMR spectroscopy experiments. Thus, solutions of (*E*)-**VC1801** in deuterated methanol were initially prepared in two separate Pyrex NMR tubes and analyzed by ^{1}H NMR spectroscopy (t = 0). In order to evaluate the role played of the ambient oxygen, the solutions were then carefully concentrated under a nitrogen stream to afford amorphous solids of compound (*E*)-**VC1801**. One NMR tube was left open (open tube experiment, OTE) to allow the film to be exposed to atmospheric oxygen, and to reproduce the conditions used in the above-described irradiation studies. On the other hand, the second tube was immediately sealed with an NMR tube cap (sealed tube experiment, STE) in the attempt of excluding the presence of oxygen into the film. Both samples were irradiated under continuous rotation for 24 h in a UV-A chamber

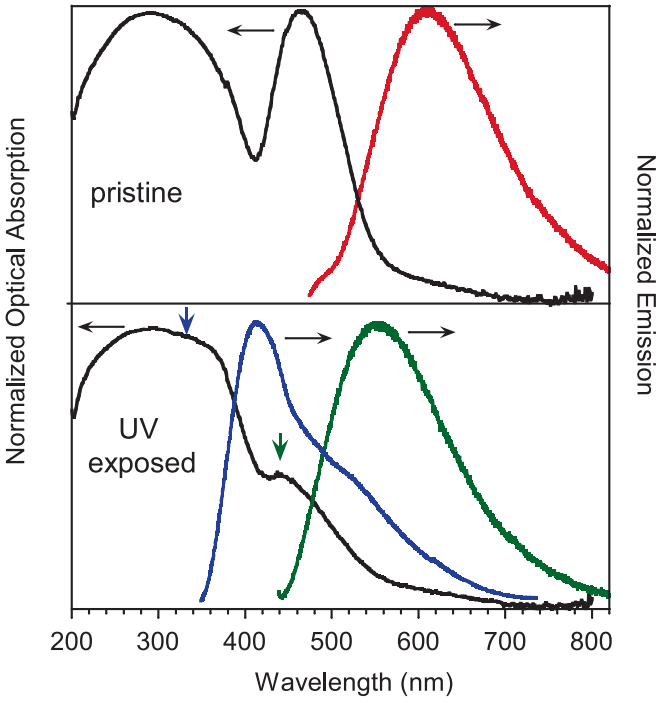


Fig. 9. Normalized absorption (black lines) and PL spectra of a (*E*)-**VC1801** cast film deposited from methanol solution before (top) and after 150 min of irradiation of the film at 330 nm (bottom). PL spectra of the pristine film were obtained at λ_{ex} = 450 nm (top, red line), and the vertical arrows indicate the excitation wavelengths for the irradiated film (bottom, λ_{ex} = 330 nm blue line; λ_{ex} = 440 nm, green line).

equipped with two G15T8 Hg UV-A lamps (2 × 15 W) since the optical

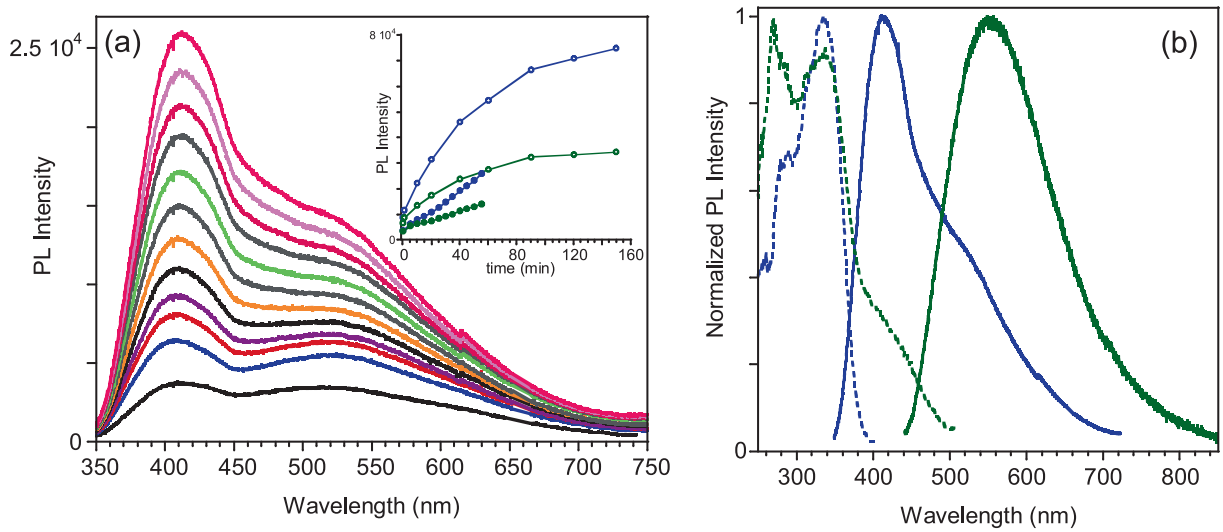


Fig. 10. (a) Effect of the first irradiation cycle (λ_{ex} = 330 nm, 3 mW/cm^2) on the PL of a cast film of (*E*)-**VC1801** (each spectrum was recorded after 5 min exposure, from bottom to top). The inset shows the PL intensity at λ_{em} = 412 nm (blue) and λ_{em} = 525 nm (green) in the first (0–55 min, solid squares) and second (0–150 min, open squares) irradiation cycle. (b) PL (solid lines) and PLE (dashed lines) of a cast film of (*E*)-**VC1801** after the second cycle of irradiation at 330 nm. λ_{ex} = 330 nm (blue) and λ_{ex} = 440 nm (green); λ_{em} = 412 nm (blue) and λ_{em} = 525 nm (green).

properties of compound (*E*)-**VC1801** support the use of UV-A region. After irradiation, the amorphous solids were redissolved in deuterated methanol and analyzed by ^{1}H NMR spectroscopy to evaluate the effects of the photochemical treatment (Fig. 11).

The comparison of the resulting ^{1}H NMR spectra with that of the starting (*E*)-**VC1801** suggested that along with the photoisomerization

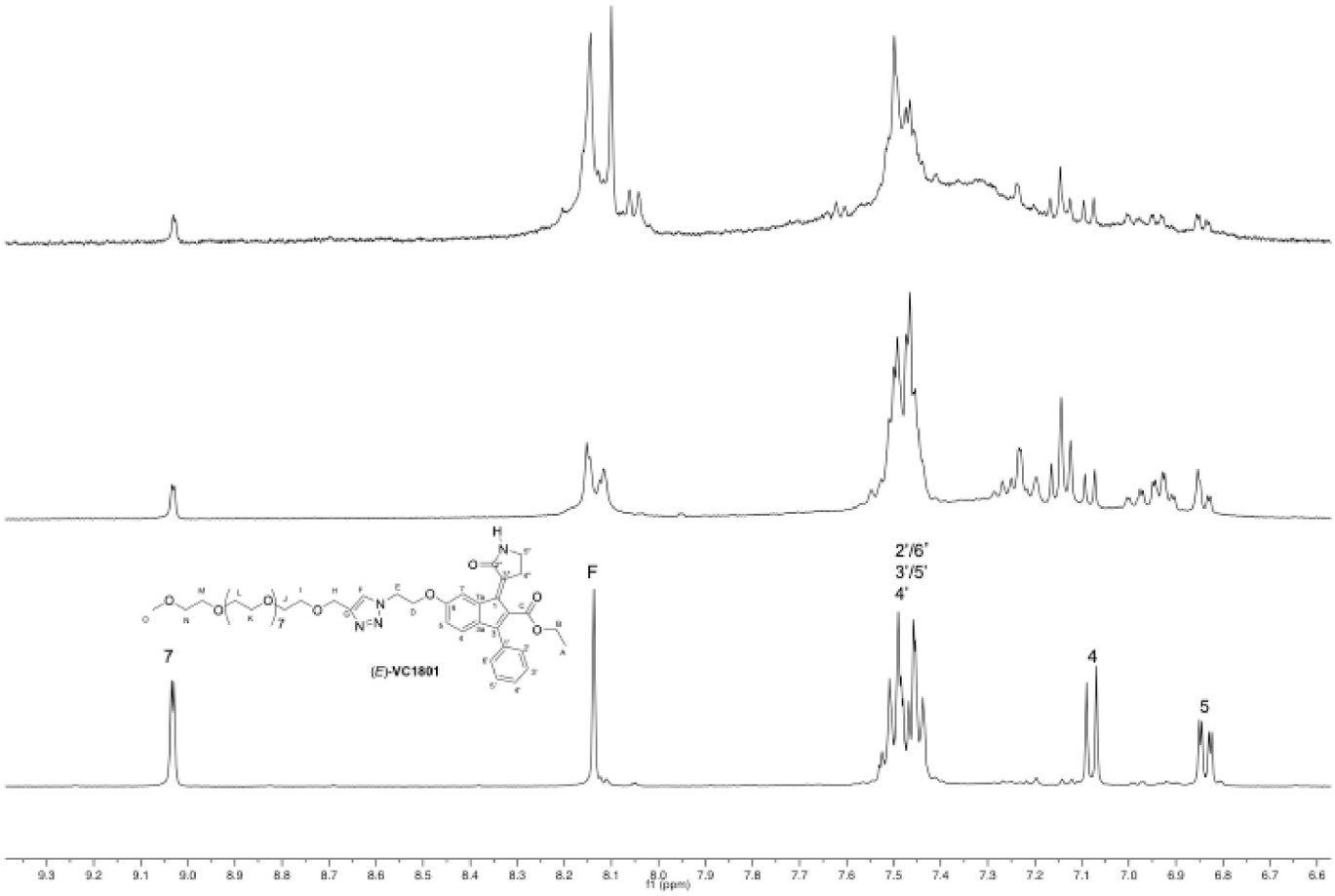


Fig. 11. Comparison of the aromatic regions of the ^{1}H NMR spectra (400 MHz, CD_3OD) recorded after irradiating amorphous solids of (*E*)-**VC1801** with UV-A light both in the sealed tube experiment (middle trace) and in the open tube experiment (top trace). The bottom trace shows the aromatic region of the ^{1}H NMR spectrum (400 MHz, CD_3OD) obtained with starting (*E*)-**VC1801** sample.

reaction of (*E*)-**VC1801** into the corresponding (*Z*)-**VC1801**, also a polymerization process appeared to occur in both OTE and STE. Notably, the polymerization reaction appeared to be more efficient in the presence of oxygen (OTE), as the sample showed a lower residual content of monomeric (*E*)-**VC1801** and (*Z*)-**VC1801**, while the sample irradiated in the sealed tube (STE) showed a higher residual content of monomeric (*E*)-**VC1801** and (*Z*)-**VC1801**. Moreover, the photophysical features of the corresponding materials appeared to be significantly different in terms of both PL and PLE spectra (Fig. 10SI).

Thus, MALDI-TOF mass spectrometry measurements were performed to assess the differences existing in the composition of the polymeric materials obtained in the different conditions. The best mass spectra were recorded in reflectron mode using malononitrile as the matrix and are displayed in Fig. 12.

In agreement with the results observed in the polymer obtained by spontaneous polymerization, the MALDI-TOF MS spectra showed series of significant peaks at *m/z* values of around 935, 951, 953, and 967 Da with intervals equivalent to the mass of oxygen atoms. Thus, the monomeric unit of the polymer obtained by UV-A irradiation of **VC1801** films could bear one, two, or three oxygen atoms leading to sodiated ions corresponding to the mass peaks 935.5, 951.5, and 967.5, respectively (see Table 1SI). Moreover, the analysis of the peaks corresponding to dimeric and trimeric species confirmed the presence of sequences showing lower oxygen contents with respect to those expected for an alternated co-polymer. FT-IR analysis (Fig. 1SI, spectra b and c) confirmed the presence of the peroxide bond and the different oxidation degree of the two samples. In fact, the intensity of the bands at 1130, 1000, and 950 cm^{-1} increased with the relative amount of peroxide bond in the copolymer chains. These results confirmed the tendency of benzofulvene derivative **VC1801** to copolymerize with molecular oxygen to afford random copolymer materials containing homo-polymeric sequences. The attempts done in excluding molecular oxygen from the film during the irradiation experiments (i. e. STE) failed in providing the homo-polymer, but as already observed by NMR studies, they depressed the polymerization reaction. These results appeared to suggest that the formation of poly-**VC1801** homo-polymer could be hindered by steric hindrance reasons, which could be mitigated by the intercalation of molecular oxygen also when present in low amount as in STE. However, the difference in the emission features observed in the polymer samples obtained by UV-A irradiation of **VC1801** films in the presence/absence of atmospheric oxygen supported the existence of differences in the chemical composition of the samples. These differences are visible in the MALDI-TOF spectra (Fig. 12), which allowed us to assume the existence of different oxidation degrees in the two polymeric samples. In other words, the two poly-**VC1801** samples could differ for their content in homo-polymer sequences.

Conclusion

Recently, we described GFP-related chromophores based on a 3-phenylbenzofulvene scaffold capable of absorbing visible light and photoisomerizing in the picosecond time scale, and in which aggregation appeared to affect the photochemical features.

These compounds were found to be stable in the ordered crystalline state, but in the disordered amorphous state, (*E*)-**VC1801** appeared to undergo spontaneous polymerization to provide random copolymer materials containing homo-polymer sequences along with those in which the polybenzofulvene monomeric units are intercalated with molecular oxygen as in an alternate co-polymer.

The aggregation propensity of (*E*)-**VC1801** leading to the formation of micelles in water provided us with the opportunity of characterizing the aggregation process by NMR spectroscopy and dynamic light scattering (DLS) techniques. Thus, in the present work, these techniques were employed to gain information about the self-assembling process in the relatively disordered state in which polymerization appeared to occur. These studies highlighted the importance of the specific aromatic interaction in the aggregation process of (*E*)-**VC1801**.

The interaction of benzofulvene derivative (*E*)-**VC1801** with light was studied both from the point of view of the photophysical and photochemical features. Interestingly, the optical features of this benzofulvene molecular switch differed deeply on the bases of its aggregation state. In particular, the photophysical features of (*E*)-**VC1801** molecularly dispersed in methanol were moderately affected by the irradiation with UV-A light, and ^{1}H NMR experiments demonstrated that

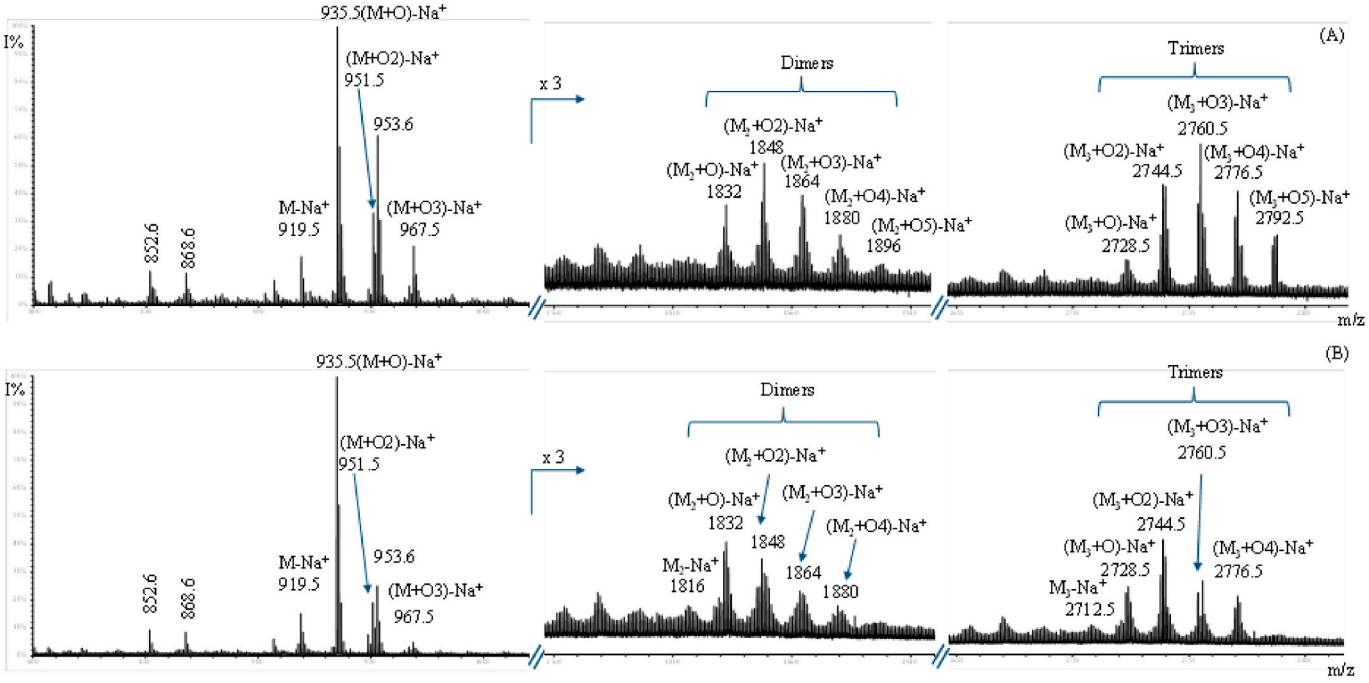


Fig. 12. Comparison of the MALDI-TOF mass spectra recorded in reflectron mode using malononitrile as the matrix with the samples of poly-**VC1801** obtained by UV-A irradiation of **VC1801** in the solid state (i. e. film). Top: spectrum recorded with the polymeric material obtained in the open tube experiment. Bottom: spectrum recorded with the polymeric material obtained in the sealed tube experiment.

the irradiation of molecular dispersions produced the double-bond isomerization with the formation of the corresponding (*Z*)-diastereomer.

On the other hand, in the solid state (i. e. cast films) both absorption and emission properties were strongly dependent on the UV exposure. In fact, the effect of UV irradiation on the emission properties was remarkable, suggesting that UV excitation could induce photochemical reactions in the solid state with the formation of new species (one with emission at 412 nm and one with emission at 550 nm) showing increased emission features. ^{1}H NMR analysis of the irradiated films showed that along with the photoisomerization reaction of (*E*)-**VC1801** into the corresponding (*Z*)-**VC1801**, also a polymerization process appeared to occur. Moreover, the polymerization reaction was more efficient in the presence of atmospheric oxygen than in the sample irradiated under a reduced oxygen content, and the photophysical features of the corresponding polymeric materials appeared to be significantly different in terms of both PL and PLE spectra. These differences in the emission features supported the existence of differences in the composition of the samples such as their content in homo-polymer sequences.

EXPERIMENTAL SECTION

NMR spectroscopy studies. The NMR spectra were recorded with a Bruker DRX-400 AVANCE, or a Bruker DRX-600 AVANCE III spectrometers. The proton NMR experiments were performed at 298.0 K accumulating 128 FIDs with 16 K data points and a spectral width of 8 kHz. A 90° excitation pulse (8.0 μs) was used with a relaxation delay of 1.5 s.

The spin–lattice relaxation rates (R_1) were measured using the (180°-τ-90°-t)$_n$ sequence. The τ values used for non-selective experiments were the following: 0.01, 0.02, 0.04, 0.06, 0.08, 0.1, 0.2, 0.4, 0.8, 1, 1.4, 2, 3, 4, 5, 8, 20 s respectively, and the delay time (t) was 20 s. The maximum experimental error in the relaxation rate measurements was 5 %.

The NOESY experiments were acquired using the NOESYESGPPH sequence (Nuclear Overhauser Effect Spectroscopy with excitation sculpting using gradients and phase cycling), which represents one of the most widely employed variants of two-dimensional experiments for samples in aqueous solution, particularly when efficient water signal suppression is required. This sequence combines the classical three π/2 pulse scheme of two-dimensional NOESY with an excitation sculpting module based on field gradients and selective pulses, enabling more efficient and less perturbing water suppression compared to traditional methods. The acquisition parameters consisted of 2048 points in the direct dimension and 256 complex points in the indirect dimension, with three different mixing time (200, 400 and 600 ms).

All NMR experiments were processing with MestReNova software.

Matrix assisted laser desorption/ionization time of flight (MALDI-TOF) mass spectra were recorded by a 4800 Proteomic Analyzer (Applied Biosystems, MA, USA) MALDI-TOF/TOF instrument equipped with a Nd:YAG laser at a wavelength of 355 nm with < 500 ps pulse and 200 Hz firing rate, operating in reflectron mode. The accelerating voltage was 15 kV. External calibration was performed using an Applied Biosystems calibration mixture consisting of polypeptides with different molar mass values. The irradiance was maintained slightly above the threshold to obtain a mass resolution of about 4000–6000 fwhm. Mass accuracy was about 50 ppm. Several matrices [i. e. 1,8,9-anthracenetriol (dithranol); α-Cyano-4-hydroxycinnamic acid (CHCA); *trans*-2-[3-(4-*tert*-butylphenyl)-2-methyl-2-propenylidene]malononitrile (malononitrile); *trans*-3-indoleacrylic acid (IAA)] were used. The best mass spectra were recoded using malononitrile o dithranol as a matrix.

Differential Scanning Calorimetry (DSC) measurements were carried out by a TA Instruments Q100 DSC calorimeter. The instrument was calibrated evaluating the melt purity of an Indium standard (156.6 °C and 28.45 J/g). samples were heated from −90 °C up to 160 °C with a heating rate of 10 °C/min, under N_2 flow (50 mL/min).

Fourier Transform Infrared (FT-IR) spectra were recorded by a Perkin-Elmer Instruments (Milan, Italy), the Spectrum One FT-IR Spectrometer having a lithium tantalate (LiTaO3) single crystal detector. The spectra were acquired in the Middle Infrared (4000–400 cm^{-1}) in modality transmittance and processed through the software Spectrum One. Anhydrous KBr pellets of each sample (1 %w) were accurately prepared under vacuum using an evacuable Pellet Die system and hydraulic press applying a p of 5 tons of 1 min.

Size exclusion Chromatography (SEC) were performed by a SEC Azura P6.1 apparatus (made in Germany) equipped with precolumn TSKgel guard Super H-L (982 T) ad five TSKgel Super H columns (H5000, H4000, H3000, H2500 and H1000) − 6.0 mm ID x 150 mm, using THF as solvent (1.0 ml/min). The SEC curves were elaborated with the program Clarity.

Dynamic light scattering (DLS). Particle size distribution and polydispersity index were determined using a Zetasizer Ultra RED system (Malvern, UK) with a backscatter (173°) detector angle. All samples were measured in triplicate. Analysis of results was performed by ZS Explorer software by Malvern Panalytical, that employs Cumulants analysis.

Photophysical characterization studies. UV–vis absorption spectra are obtained with a Perkin Elmer Lambda 900 spectrometer. PL spectra are obtained with NanoLog composed by a iH320 spectrograph equipped with a Synapse QExtra charge-coupled device, by exciting with a 450 W Xe lamp monochromated with a double grating Gemini 180. The spectra are corrected for the instrument response. Irradiation at 330 nm is performed by exposure to the Xe lamp light monochromated (slit 2 mm) with a Gemini 180 double monochromator.

Photochemical characterization studies in solution. Solutions of (*E*)-**VC1801** in CD_3OD contained into 5 mm NMR Pyrex tubes were irradiated with a monochromatic light centered at the appropriate wavelength (330, 360, and 460 nm) by mean of a tunable light source Zolix (TLS2-X300PU-G, 300 W UV Xenon Light Source with monochromator Omni-λ2047i) at room temperature for the suitable time while ^{1}H NMR spectra were recorded at regular time intervals to ascertain the effects of the irradiation.

Photochemical characterization studies in the solid state. Solutions of (*E*)-**VC1801** in deuterated methanol were initially prepared into separate 5 mm NMR Pyrex tubes and analyzed by ^{1}H NMR spectroscopy (t = 0). The solutions were then carefully concentrated under a nitrogen stream to afford amorphous solids of compound (*E*)-**VC1801**. Some NMR tubes were left open to allow the exposure to atmospheric oxygen, whereas some other tubes were immediately sealed with NMR tube caps to allow the experiment to be conducted under oxygen-free conditions. The samples were irradiated in a UV-A Multyrays chamber equipped with two G15T8 Hg UV-A tubes (2 x 15 Watt) under continuous rotation for 24 h. After irradiation, the amorphous solids were redissolved in deuterated methanol and analyzed by ^{1}H NMR spectroscopy.

CRediT authorship contribution statement

Alessandro Donati: Investigation. **Claudia Bonechi:** Investigation. **Jacopo Venditti:** Investigation. **Marco Paolino:** Investigation. **Mario Saletti:** Investigation. **Germano Giuliani:** Investigation. **Gianluca Giorgi:** Investigation. **Giuseppa Mercorillo:** Investigation. **Filippo Samperi:** Investigation. **Chiara Botta:** Writing – original draft, Investigation. **Andrea Cappelli:** Writing – review & editing, Writing – original draft, Supervision, Project administration.

Declaration of competing interest

The authors declare that they have no known competing financial interests or personal relationships that could have appeared to influence the work reported in this paper.

Appendix A. Supplementary data

Supplementary data to this article can be found online at https://doi.org/10.1016/j.eurpolymj.2026.115033.

Data availability

Data will be made available on request.

References

[1] M. Hasegawa, Photopolymerization of diolefin crystals, Chem. Rev. 83 (5) (1983) 507–518, https://doi.org/10.1021/cr00057a001.

[2] K. Biradha, R. Santra, Crystal engineering of topochemical solid state reactions, Chem. Soc. Rev. 42 (3) (2013) 950–967, https://doi.org/10.1039/C2CS35343A.

[3] Hasegawa, M. Photodimerization and photopolymerization of diolefin crystals, in: D.B.T.-A. in P.O.C. Bethell (Ed.), Academic Press, 1995: pp. 117–171. DOI:10.1016/S0065-3160(08)60034-9.

[4] D. Letian, Z. Yonghao, S. Xiaoqin, W. Guang, F. Kirk, H. Wan-Ching, Z. Huanping, Y. Yang, W. Fred, Single-crystal linear polymers through visible light–triggered topochemical quantitative polymerization, Science 343 (6168) (2014) 272–277, https://doi.org/10.1126/science.1245875.

[5] R. Mohanrao, K. Hema, K.M. Sureshan, Topochemical synthesis of different polymorphs of polymers as a paradigm for tuning properties of polymers, Nat. Commun. 11 (2020) 865, https://doi.org/10.1038/s41467-020-14733-y.

[6] L. Peng, Q. Guo, C. Song, S. Ghosh, H. Xu, L. Wang, D. Hu, L. Shi, L. Zhao, Q. Li, T. Sakurai, H. Yan, S. Seki, Y. Liu, D. Wei, Ultra-fast single-crystal polymerization of large-sized covalent organic frameworks, Nat. Commun. 12 (2021) 5077, https://doi.org/10.1038/s41467-021-24842-x.

[7] Q. Yu, M. Li, J. Gao, P. Xu, Q. Chen, D. Xing, J. Yan, M.J. Zaworotko, J. Xu, Y. Chen, P. Cheng, Z. Zhang, Fabrication of large single crystals for platinum-based linear polymers with controlled-release and photoactuator performance, Angew. Chemie Int. Ed. 58 (51) (2019) 18634–18640, https://doi.org/10.1002/anie.201910749.

[8] T. Niu, C. Hua, M. Zhou, On-surface synthesis toward two-dimensional polymers, J. Phys. Chem. Lett. 13 (34) (2022) 8062–8077, https://doi.org/10.1021/acs.jpclett.2c01481.

[9] A. Matsumoto, T. Tanaka, T. Tsubouchi, K. Tashiro, S. Saragai, S. Nakamoto, Crystal engineering for topochemical polymerization of muconic esters using halogen−halogen and CH/π interactions as weak intermolecular interactions, J. Am. Chem. Soc. 124 (30) (2002) 8891–8902, https://doi.org/10.1021/ja0205333.

[10] J.-M. Heo, Y. Kim, S. Han, J.F. Joung, S. Lee, S. Han, J. Noh, J. Kim, S. Park, H. Lee, Y.M. Choi, Y.-S. Jung, J.-M. Kim, Chromogenic tubular polydiacetylenes from topochemical polymerization of self-assembled macrocyclic diacetylenes, Macromolecules 50 (3) (2017) 900–913, https://doi.org/10.1021/acs.macromol.6b02493.

[11] J. Fan, X. Xu, W. Yu, Z. Wei, D. Zhang, Hydrogen-bond-driven supramolecular self-assembly of diacetylene derivatives for topochemical polymerization in solution, Polym. Chem. 11 (2020) 1947–1953, https://doi.org/10.1039/C9PY01745C.

[12] E. Jahnke, I. Lieberwirth, N. Severin, J.P. Rabe, H. Frauenrath, Topochemical polymerization in supramolecular polymers of oligopeptide-functionalized diacetylenes, Angew. Chemie Int. Ed. 45 (32) (2006) 5383–5386, https://doi.org/10.1002/anie.200600610.

[13] A. Cappelli, G. Pericot-Mohr, M. Anzini, S. Vomero, A. Donati, M. Casolaro, R. Mendichi, G. Giorgi, F. Makovec, Synthesis and characterization of a new benzofulvene polymer showing a thermoreversible polymerization behaviour, J. Org. Chem. 68 (24) (2003) 9473–9476, https://doi.org/10.1021/jo035104h.

[14] A. Cappelli, M. Anzini, S. Vomero, A. Donati, L. Zetta, R. Mendichi, M. Casolaro, P. Lupetti, P. Salvatici, G. Giorgi, New π-stacked benzofulvene polymer showing thermoreversible polymerization: Studies in macromolecular and aggregate structures and polymerization mechanism. *J. Polym. Sci. Part a*, Polym. Chem. 43 (15) (2005) 3289–3304, https://doi.org/10.1002/pola.20783.

[15] A. Cappelli, S. Galeazzi, G. Giuliani, M. Anzini, A. Donati, L. Zetta, R. Mendichi, M. Aggravi, G. Giorgi, E. Paccagnini, S. Vomero, Structural manipulation of benzofulvene derivatives showing spontaneous thermoreversible polymerization. Role of the substituents in the modulation of polymer properties, Macromolecules 40 (5) (2007) 3005–3014, https://doi.org/10.1021/ma0629236.

[16] A. Cappelli, S. Galeazzi, G. Giuliani, M. Anzini, M. Aggravi, A. Donati, L. Zetta, A. C. Boccia, R. Mendichi, G. Giorgi, E. Paccagnini, S. Vomero, Anionic polymerization of a benzofulvene monomer leading to a thermoreversible π-stacked polymer. Studies in macromolecular and aggregate structure, Macromolecules 41 (7) (2008) 2324–2334, https://doi.org/10.1021/ma702319h.

[17] A. Cappelli, S. Galeazzi, G. Giuliani, M. Anzini, M. Grassi, R. Lapasin, G. Grassi, R. Farra, B. Dapas, M. Aggravi, A. Donati, L. Zetta, A.C. Boccia, F. Bertini, F. Samperi, S. Vomero, Synthesis and spontaneous polymerization of oligo (ethylene glycol)-conjugated benzofulvene macromonomers. A polymer brush forming a physical hydrogel, Macromolecules 42 (7) (2009) 2368–2378, https://doi.org/10.1021/ma802429g.

[18] A. Cappelli, M. Paolino, P. Anzini, G. Giuliani, S. Valenti, M. Aggravi, A. Donati, R. Mendichi, L. Zetta, A.C. Boccia, F. Bertini, F. Samperi, S. Battiato, E. Paccagnini, S. Vomero, Structure-property relationships in densely grafted π-stacked polymers. J. Polym. Sci. Part A Polym. Chem. 48 (11) (2010) 2446–2461, https://doi.org/10.1002/pola.24016.

[19] A. Cappelli, M. Paolino, G. Grisci, G. Giuliani, A. Donati, R. Mendichi, A.C. Boccia, F. Samperi, A click chemistry-based "' grafting through "' approach to the synthesis of a biorelevant polymer brush, Polym. Chem. 2 (11) (2011) 2518–2527, https://doi.org/10.1039/c1py00271f.

[20] A. Cappelli, M. Paolino, G. Grisci, G. Giuliani, A. Donati, R. Mendichi, A.C. Boccia, C. Botta, W. Mróz, F. Samperi, A. Scamporrino, G. Giorgi, S. Vomero, Synthesis and characterization of charge-transporting π-stacked polybenzofulvene derivatives, J. Mater. Chem. 22 (2012) 9611–9623, https://doi.org/10.1039/c2jm16790e.

[21] A. Cappelli, G. Grisci, M. Paolino, F. Castriconi, G. Giuliani, A. Donati, S. Lamponi, R. Mendichi, A.C. Boccia, F. Samperi, S. Battiato, E. Paccagnini, M. Gentile, M. Licciardi, G. Giammona, S. Vomero, Combining spontaneous polymerization and click reactions for the synthesis of polymer brushes: A "grafting onto" approach, Chem Eur J 19 (29) (2013) 9710–9721, https://doi.org/10.1002/chem.201202534.

[22] A. Cappelli, F. Villafiorita-Monteleone, G. Grisci, M. Paolino, V. Razzano, G. Fabio, G. Giuliani, A. Donati, R. Mendichi, A.C. Boccia, M. Pasini, C. Botta, Highly emissive supramolecular assemblies based on π-stacked polybenzofulvene hosts and a benzothiadiazole guest, J. Mater. Chem. C 2 (2014) 7897–7905, https://doi.org/10.1039/C4TC01200C.

[23] Cappelli, A.; Paolino, M.; Grisci, G.; Giuliani, G.; Donati, A.; Boccia, A. C.; Samperi, F.; Mendichi, R.; Vomero, S. Reversible polymerization techniques leading to π-stacked polymers., in: T. Nakano (Ed.), π-Stacked Polym. Mol., Ed., Sprin, Springer Japan, Japan: Osaka, 2014: pp. 51–149. DOI:10.1007/978-4-431-54129-5_2.

[24] A. Cappelli, G. Grisci, M. Paolino, V. Razzano, G. Giuliani, A. Donati, C. Bonechi, R. Mendichi, A.C. Boccia, M. Licciardi, C. Scialabba, G. Giammona, S. Vomero, Polybenzofulvene derivatives bearing dynamic binding sites as potential anticancer drug delivery systems, J. Mater. Chem. B 3 (2015) 361–374, https://doi.org/10.1039/c4tb01268b.

[25] F. Villafiorita-Monteleone, A. Cappelli, M. Paolino, M. Colombo, E. Cariati, A. Mura, G. Bongiovanni, C. Botta, Aggregation-induced Förster resonance energy transfer in polybenzofulvene/dye nanoparticles, J. Phys. Chem. C 119 (33) (2015) 18986–18991, https://doi.org/10.1021/acs.jpcc.5b05589.

[26] A. Cappelli, V. Razzano, M. Paolino, G. Grisci, G. Giuliani, A. Donati, R. Mendichi, F. Samperi, S. Battiato, A.C. Boccia, A. Mura, G. Bongiovanni, W. Mróz, C. Botta, Bithiophene-based polybenzofulvene derivatives with high stacking and hole mobility, Polym. Chem. 6 (42) (2015) 7377–7388, https://doi.org/10.1039/C5PY00904A.

[27] A. Cappelli, V. Razzano, G. Fabio, M. Paolino, G. Grisci, G. Giuliani, A. Donati, R. Mendichi, W. Mróz, F. Villafiorita-Monteleone, C. Botta, Side chain engineering in π-stacked polybenzofulvene derivatives bearing electron-rich chromophores for OLED applications, RSC Adv. 5 (123) (2015) 101377–101385, https://doi.org/10.1039/c5ra21164f.

[28] W. Mróz, F. Villafiorita-Monteleone, M. Pasini, G. Grisci, M. Paolino, V. Razzano, A. Cappelli, C. Botta, π-Stacked polybenzofulvene derivatives as hosts for yellow and red emitting OLEDs, Mater. Lett. 142 (2015) 197–200, https://doi.org/10.1016/j.matlet.2014.12.002.

[29] A. Cappelli, M. Paolino, G. Grisci, V. Razzano, G. Giuliani, A. Donati, C. Bonechi, R. Mendichi, S. Battiato, F. Samperi, C. Scialabba, G. Giammona, F. Makovec, M. Licciardi, Hyaluronan-coated polybenzofulvene brushes as biomimetic materials, Polym. Chem. 7 (2016) 6529–6544, https://doi.org/10.1039/C6PY01644H.

[30] F. Villafiorita-Monteleone, E. Kozma, M. Pasini, M. Paolino, A. Cappelli, G. Bongiovanni, A. Mura, C. Botta, Polybenzofulvenes-based blends with benzothiadiazole and perylene diimide derivatives emitting from yellow to the deep-red by resonant energy transfer processes, Appl. Phys. Lett. 110 (18) (2017) 183301, https://doi.org/10.1063/1.4983022.

[31] F. Fabrizi de Biani, A. Reale, V. Razzano, M. Paolino, G. Giuliani, A. Donati, G. Giorgi, W. Mróz, D. Piovani, C. Botta, A. Cappelli, Electrochemical and optoelectronic properties of terthiophene- and bithiophene-based polybenzofulvene derivatives, RSC Adv. 8 (2018) 10836–10847, https://doi.org/10.1039/c7ra13242e.

[32] F. Villafiorita-Monteleone, E. Kozma, U. Giovanella, M. Catellani, M. Paolino, V. Collico, M. Colombo, A. Cappelli, C. Botta, Red and deep-red emissive polymeric nanoparticles based on polybenzofulvene and perylenediimide derivatives, Dye. Pigment. 149 (2018) 331–335, https://doi.org/10.1016/j.dyepig.2017.10.010.

[33] M. Paolino, G. Grisci, A. Reale, V. Razzano, G. Giuliani, A. Donati, R. Mendichi, D. Piovani, A.C. Boccia, A. Grillo, G. Giorgi, A. Cappelli, Structural manipulation of the conjugated phenyl moiety in 3-phenylbenzofulvene monomers: Effects on spontaneous polymerization, Polymers 10 (7) (2018) 752, https://doi.org/10.3390/polym10070752.

[34] M. Paolino, G. Grisci, F. Castriconi, A. Reale, G. Giuliani, A. Donati, C. Bonechi, G. Giorgi, R. Mendichi, D. Piovani, A.C. Boccia, M. Canetti, F. Samperi, S. Dattilo, C. Scialabba, M. Licciardi, E. Paccagnini, M. Gentile, A. Cappelli, Densely PEGylated polybenzofulvene brushes for potential applications in drug encapsulation, Pharmaceutics 10 (4) (2018) 234, https://doi.org/10.3390/pharmaceutics10040234.

[35] M. Paolino, A. Reale, V. Razzano, G. Giuliani, A. Donati, G. Giorgi, C.A. Boccia, R. Mendichi, D. Piovani, C. Botta, L. Salvini, F. Samperi, C. Savoca, M. Licciardi, E. Paccagnini, M. Gentile, A. Cappelli, Physicochemical properties of a new PEGylated polybenzofulvene brush for drug encapsulation, Pharmaceutics 11 (9) (2019) 444, https://doi.org/10.3390/pharmaceutics11090444.

[36] M. Paolino, A. Reale, G. Magrini, V. Razzano, G. Giuliani, A. Donati, G. Giorgi, F. Samperi, M. Canetti, M. Mauro, F. Villafiorita-Monteleone, E. Fois, C. Botta,

A. Cappelli, UV-light-induced polymerization in the amorphous solid-state of a spontaneously non-polymerizing 3-phenylbenzofulvene monomer, Eur. Polym. J. 137 (2020) 109923, https://doi.org/10.1016/j.eurpolymj.2020.109923.
[37] M. Paolino, A. Reale, G. Magrini, V. Razzano, M. Saletti, G. Giuliani, A. Donati, F. Samperi, A. Scamporrino, M. Canetti, M. Mauro, F. Villafiorita-Monteleone, E. Fois, C. Botta, A. Cappelli, Synthesis and UV-light induced oligomerization of a benzofulvene-based neutral platinum(II) complex, Eur. Polym. J. 156 (2021) 110597, https://doi.org/10.1016/j.eurpolymj.2021.110597.
[38] M. Paolino, M. Saletti, A. Reale, V. Razzano, G. Giuliani, A. Donati, C. Bonechi, G. Giorgi, A. Atrei, M. Mauro, A. Scamporrino, F. Samperi, E. Fois, G. Tabacchi, C. Botta, A. Cappelli, Spontaneous polymerization of benzofulvene derivatives bearing complexed or un-complexed pyridine rings, Eur. Polym. J. 169 (2022) 111137, https://doi.org/10.1016/j.eurpolymj.2022.111137.
[39] M. Paolino, M. Saletti, A. Reale, V. Razzano, G. Giuliani, A. Donati, C. Bonechi, G. Giorgi, G. Mercorillo, F. Samperi, W. Mróz, C. Botta, A. Cappelli, Spontaneous polymerization of benzofulvene monomers bearing a 4-pyridylacetylene substituent in different positions of the benzofulvene scaffold, Eur. Polym. J. 189 (2023) 111957, https://doi.org/10.1016/j.eurpolymj.2023.111957.
[40] B.L. Feringa, N. Koumura, R.A. van Delden, M.K. ter Wiel, Light-driven molecular switches and motors, J. Appl. Phys. A 75 (2) (2002) 301–308, https://doi.org/10.1007/s003390201338.
[41] M. Baroncini, S. Silvi, A. Credi, Photo- and redox-driven artificial molecular motors, Chem. Rev. 120 (1) (2020) 200–268, https://doi.org/10.1021/acs.chemrev.9b00291.
[42] S.L. Oscurato, M. Salvatore, P. Maddalena, A. Ambrosio, From nanoscopic to macroscopic photo-driven motion in azobenzene-containing materials, Nanophotonics 7 (8) (2018) 1387–1422, https://doi.org/10.1515/nanoph-2018-0040.
[43] X. Liang, H. Nishioka, N. Takenaka, H. Asanuma, A DNA nanomachine powered by light irradiation, Chembiochem 9 (5) (2008) 702–705, https://doi.org/10.1002/cbic.200700649.
[44] C. Li, A. Iscen, L.C. Palmer, G.C. Schatz, S.I. Stupp, Light-driven expansion of spiropyran hydrogels, J. Am. Chem. Soc. 142 (18) (2020) 8447–8453, https://doi.org/10.1021/jacs.0c0220.
[45] W. Francis, A. Dunne, C. Delaney, L. Florea, D. Diamond, Spiropyran based hydrogels actuators - Walking in the light, Sensors Actuators B Chem. 250 (2017) 608–616, https://doi.org/10.1016/j.snb.2017.05.005.
[46] R.E. Dawson, S.F. Lincoln, C.J. Easton, The foundation of a light driven molecular muscle based on stilbene and α-cyclodextrin, Chem. Commun. 34 (2008) 3980–3982, https://doi.org/10.1039/b809014a.
[47] Z. Li, C. He, Z. Lu, P. Li, Y.-P. Zhu, Recent progress in all-visible-light-triggered diarylethenes, Dye. Pigment. 182 (2020) 108623, https://doi.org/10.1016/j.dyepig.2020.108623.
[48] C. Petermayer, H. Dube, Indigoid photoswitches: Visible light responsive molecular tools, Acc. Chem. Res. 51 (5) (2018) 1153–1163, https://doi.org/10.1021/acs.accounts.7b00638.
[49] J.M. Abendroth, O.S. Bushuyev, P.S. Weiss, C.J. Barrett, Controlling motion at the nanoscale: Rise of the molecular machines, ACS Nano 9 (8) (2015) 7746–7768, https://doi.org/10.1021/acsnano.5b03367.
[50] V. García-López, F. Chen, L.G. Nilewski, G. Duret, A. Aliyan, A.B. Kolomeisky, J. T. Robinson, G. Wang, R. Pal, J.M. Tour, Molecular machines open cell membranes, Nature 548 (7669) (2017) 567–572, https://doi.org/10.1038/nature23657.
[51] D. Roke, S.J. Wezenberg, B.L. Feringa, Molecular rotary motors: Unidirectional motion around double bonds, Proc. Natl. Acad. Sci. 115 (38) (2018) 94239431, https://doi.org/10.1073/pnas.1712784115.
[52] W.R. Browne, B.L. Feringa, Making molecular machines work, Nat. Nanotechnol. 1 (2006) 25–35, https://doi.org/10.1038/nnano.2006.45.
[53] J. Bauer, L. Hou, J.C.M. Kistemaker, B.L. Feringa, Tuning the rotation rate of light-driven molecular motors, J. Org. Chem. 79 (10) (2014) 4446–4455, https://doi.org/10.1021/jo500411z.
[54] J. Vicario, A. Meetsma, B.L. Feringa, Controlling the speed of rotation in molecular motors. Dramatic acceleration of the rotary motion by structural modification, Chem. Commun. 47 (2005) 5910–5912, https://doi.org/10.1039/B507264F.
[55] D. Roke, M. Sen, W. Danowski, S.J. Wezenberg, B.L. Feringa, Visible-light-driven tunable molecular motors based on oxindole, J. Am. Chem. Soc. 141 (18) (2019) 7622–7627, https://doi.org/10.1021/jacs.9b03237.
[56] M. Filatov, M. Paolino, S.K. Min, C.H. Choi, Design and photoisomerization dynamics of a new family of synthetic 2-stroke light driven molecular rotary motors, Chem. Commun. 55 (36) (2019) 5247–5250, https://doi.org/10.1039/C9CC01955C.
[57] J. Conyard, A. Cnossen, W.R. Browne, B.L. Feringa, S.R. Meech, Chemically optimizing operational efficiency of molecular rotary motors, J. Am. Chem. Soc. 136 (27) (2014) 9692–9700, https://doi.org/10.1021/ja5041368.
[58] C.T. Kornman, L. Li, A.O. Weldeab, I. Ghiviriga, K.A. Abboud, R.K. Castellano, Photoisomerization of dicyanorhodanine-functionalized thiophenes, Chem. Sci. 11 (37) (2020) 10190–10197, https://doi.org/10.1039/D0SC04409A.
[59] W.A. Velema, M.J. Hansen, M.M. Lerch, A.J.M. Driessen, W. Szymanski, B. L. Feringa, Ciprofloxacin–photoswitch conjugates: A facile strategy for photopharmacology, Bioconjug. Chem. 26 (12) (2015) 2592–2597, https://doi.org/10.1021/acs.bioconjchem.5b00591.
[60] G. Marchand, J. Eng, I. Schapiro, A. Valentini, L.M. Frutos, E. Pieri, M. Olivucci, J. Léonard, E. Gindensperger, Directionality of double-bond photoisomerization dynamics induced by a single stereogenic center, J. Phys. Chem. Lett. 6 (4) (2015) 599–604, https://doi.org/10.1021/jz502644h.
[61] M. Filatov, M. Paolino, S.K. Min, K.S. Kim, Fulgides as light-driven molecular rotary motors: Computational design of a prototype compound, J. Phys. Chem. Lett. 9 (17) (2018) 4995–5001, https://doi.org/10.1021/acs.jpclett.8b02268.
[62] S. Grunder, P.L. McGrier, A.C. Whalley, M.M. Boyle, C. Stern, J.F. Stoddart, A water-soluble pH-triggered molecular switch, J. Am. Chem. Soc. 135 (47) (2013) 17691–17694, https://doi.org/10.1021/ja409006y.
[63] C. Özçoban, T. Halbritter, S. Steinwand, L.-M. Herzig, J. Kohl-Landgraf, N. Askari, F. Groher, B. Fürtig, C. Richter, H. Schwalbe, B. Suess, J. Wachtveitl, A. Heckel, Water-soluble Py-BIPS spiropyrans as photoswitches for biological applications, Org. Lett. 17 (6) (2015) 1517–1520, https://doi.org/10.1021/acs.orglett.5b00397.
[64] S. Ludwanowski, M. Ari, K. Parison, S. Kalthoum, P. Straub, N. Pompe, S. Weber, M. Walter, A. Walther, pH tuning of water-soluble arylazopyrazole photoswitches, Chem Eur J 26 (58) (2020) 13203–13212, https://doi.org/10.1002/chem.202000659.
[65] J. Léonard, I. Schapiro, J. Briand, S. Fusi, R. Rossi Paccani, M. Olivucci, S. Haacke, Mechanistic origin of the vibrational coherence accompanying the photoreaction of biomimetic molecular switches, Chem Eur J 18 (2012) 15296–15304, https://doi.org/10.1002/chem.201201430.
[66] M. Gueye, M. Paolino, E. Gindensperger, S. Haacke, M. Olivucci, J. Léonard, Vibrational coherence and quantum yield of retinal-chromophore-inspired molecular switches, Faraday Discuss. 221 (2020) 299–321, https://doi.org/10.1039/c9fd00062c.
[67] M. Gueye, M. Manathunga, D. Agathangelou, Y. Orozco, M. Paolino, S. Fusi, S. Haacke, M. Olivucci, J. Léonard, Engineering the vibrational coherence of vision into a synthetic molecular device, Nat. Commun. 9 (1) (2018) 313, https://doi.org/10.1038/s41467-017-02668-w.
[68] K. Pagano, M. Paolino, S. Fusi, V. Zanirato, C. Trapella, G. Giuliani, A. Cappelli, S. Zanzoni, H. Molinari, L. Ragona, M. Olivucci, Bile acid binding protein functionalization leads to a fully synthetic rhodopsin mimic, J. Phys. Chem. Lett. 10 (9) (2019) 2235–2243, https://doi.org/10.1021/acs.jpclett.9b00210.
[69] I. Schapiro, M. Gueye, M. Paolino, S. Fusi, G. Marchand, S. Haacke, M.E. Martin, M. Huntress, V.P. Vysotskiy, V. Veryazov, J. Léonard, M. Olivucci, Synthesis, spectroscopy and QM/MM simulations of a biomimetic ultrafast light-driven molecular motor, Photochem. Photobiol. Sci. 18 (9) (2019) 2259–2269, https://doi.org/10.1039/C9PP00223E.
[70] M. Paolino, M. Gueye, E. Pieri, M. Manathunga, S. Fusi, A. Cappelli, L. Latterini, D. Pannacci, M. Filatov, J. Léonard, M. Olivucci, Design, Synthesis, and dynamics of a green fluorescent protein fluorophore mimic with an ultrafast switching function, J. Am. Chem. Soc. 138 (31) (2016) 9807–9825, https://doi.org/10.1021/jacs.5b10812.
[71] M. Paolino, T. Giovannini, M. Manathunga, L. Latterini, G. Zampini, R. Pierron, J. Léonard, S. Fusi, G. Giorgi, G. Giuliani, A. Cappelli, C. Cappelli, M. Olivucci, On the transition from a biomimetic molecular switch to a rotary molecular motor, J. Phys. Chem. Lett. 12 (16) (2021) 3875–3884, https://doi.org/10.1021/acs.jpclett.1c00526.
[72] N. Ferrara, G. Giuliani, M. Maimaris, S. Prioli, M. Manathunga, L. Blancafort, J. Léonard, A. Cappelli, M. Olivucci, M. Paolino, Design, Synthesis, and Characterization of pH-resettable Photoswitches Mimicking the GFP Fluorophore Structure, J. Phys. Chem. B 129 (2025) 2845–2855, https://doi.org/10.1021/acs.jpcb.4c07003.
[73] M. Paolino, M. Saletti, A. Reale, M. Licciardi, P. Varvarà, A. Marquette, J. Léonard, C. Bonechi, A. Donati, G. Giorgi, G. Giuliani, B. Carlotti, F. Ortica, L. Latterini, M. Gentile, E. Paccagnini, M. Olivucci, A. Cappelli, Design, synthesis and characterization of a visible-light-sensitive molecular switch and its PEGylation towards a self-assembling molecule, Chem Eur J 28 (50) (2022) e202201477, https://doi.org/10.1002/chem.202201477.
[74] T. Nakano, O. Nakagawa, T. Yade, Y. Okamoto, Solid-state polymerization of dibenzofulvene leading to a copolymer with oxygen, Macromolecules 36 (5) (2003) 1433–1435, https://doi.org/10.1021/ma025792r.
[75] S.R.K. Alinas, The application of solution NMR spectroscopy to study dynamics of two-domain calcium-binding proteins, J. Magnetic Resonance Open 16–17 (2023) 100120, https://doi.org/10.1016/j.jmro.2023.100120.
[76] A.A. Kawale, B.M. Burmann, Chapter 5 - Advanced NMR spectroscopy methods to study protein structure and dynamics, in: In Advanced Spectroscopic Methods to Study Biomolecular Structure and Dynamics, 2023, pp. 125–152, https://doi.org/10.1016/B978-0-323-99127-8.00010-6.